nanomanufacturing

MDPI

Review

Progress and Challenges of Chloride–Iodide Perovskite Solar Cells: A Critical Review

Ashraful Hossain Howlader * and Ashraf Uddin *

School of Photovoltaic and Renewable Energy Engineering, University of New South Wales, Sydney, NSW 2052, Australia

* Correspondence: a.howlader@unsw.edu.au (A.H.H.); a.uddin@unsw.edu.au (A.U.)

Abstract: Chloride–iodide perovskites have received substantial interest due to their better photovoltaic performance compared to pure iodide ones. The superior properties of chloride–iodide perovskites boost photovoltaic performance. However, quantifying the Cl composition in perovskite films remains challenging. Hence, it is not easy to correlate the Cl quantity with the improved photovoltaic performance. Considering this critical issue, it is still necessary to determine the correlation between the Cl quantity and the improved photovoltaic performance to solve this puzzle. Here, a critical review is presented showcasing the significant impacts of the Cl quantity on chloride–iodide perovskites and related solar cell devices. This review provides an up-to-date picture of different strategic methods to overcome the challenges of Cl incorporation in I-based perovskites, aiming to improve photovoltaic performance. Finally, some valuable remedies are prescribed for potential future research strategies to study the photovoltaic performance of chloride–iodide perovskite solar cells. Hopefully, this review will be a noteworthy scientific contribution to the advancement of the continuous progress of perovskite solar cells.

Keywords: perovskite solar cells; chloride–iodide perovskites; efficiency; stability

Citation: Howlader, A.H.; Uddin, A. Progress and Challenges of Chloride–Iodide Perovskite Solar Cells: A Critical Review. *Nanomanufacturing* **2023**, *3*, 177–216. https://doi.org/10.3390/nanomanufacturing3020012

Academic Editor: Christian Julien

Received: 7 April 2023
Revised: 1 May 2023
Accepted: 3 May 2023
Published: 15 May 2023

1. Introduction

Over the last decade, many researchers have conducted extensive studies on perovskite solar cells (PSCs). In particular, lead halide PSCs have established a firm foothold in the path of their continuous progress. This is due to their gradually increasing power conversion efficiency (PCE), approaching that of conventional inorganic semiconductors. Additionally, lead halide perovskites facilitate low-cost solution process photovoltaic technology, making them a strong competitor to commercially available silicon-based solar cells [1]. PSCs came into the limelight as a solid-state form in 2012, having a PCE of about 9% [2]. Now, the PCE of PSCs in 2023 is more than 25% [3].

The perovskite layer plays all the major roles of photovoltaic operation, such as light absorption, electron–hole pair generation, the transport of photogenerated electrons and holes toward the corresponding electrodes, etc. Therefore, controlling perovskites' optoelectronic and morphological properties is essential to make high-performance solar cells.

It has been well established that, as the primitive material in PSCs, $MAPbI_3$ has excellent optical absorption properties with a suitable bandgap of about 1.55 eV to absorb visible light, a balanced carrier diffusion length, and a remarkable carrier lifetime. These superior properties confirm the superb performance of these PSCs [4]. Although most PSCs are based on $MAPbI_3$ due to the above advantages, there is a great concern about the widespread use of Pb in PSCs for long-term environmental sustainability [5]. In this regard, researchers have suggested a few alternative metal cations. To date, one of the most suitable candidates considered to replace Pb is Sn, which is less toxic and has fewer environmental impacts [6,7]. Sn-based perovskite is much more unstable than Pb-based

perovskite. Sn is oxidized by oxygen, and Sn-based perovskite degrades too quickly in ambient conditions. This is one of the reasons for choosing Pb-based PSCs. There are also other possible alternative candidates, such as Bi, In, Sr, Cd, Ca, etc. [8,9].

The bandgap of halide perovskite is determined by metal cation and halide anion orbital couplings. Different halide ion combinations change the perovskite lattice to enhance or reduce wavefunction overlapping and result in different bandgaps. Generally, perovskites with a bandgap greater than 1.65 eV are defined as wide-bandgap perovskites. Introducing bromide ions with iodide ions is a common strategy for making wide-bandgap perovskites [10]. Higher-bandgap perovskites cut out most of the solar spectrum in the longer-wavelength region. Therefore, higher-bandgap PSCs are not suitable for single-junction solar cells. It is observed that introducing a trace quantity of Cl can dramatically improve the optoelectrical and morphological properties while maintaining a bandgap similar to that of $MAPbI_3$. For example, the electron diffusion length is almost ten times longer [11]; the carrier lifetime is substantially prolonged to 1 μs [12]; and the grain size increases to the range of μm from the nm scale [13]. Some interesting phenomena in chloride–iodide perovskite are absent in iodide perovskite. For example, there is less I^- ion migration, and Cl^- ions migrate toward the interface with the electron transport layer. It is well known that there is a significant difference in radius between Cl and I. Cl is much smaller than I. Due to its smaller size, it is quite challenging to incorporate Cl into I-perovskite. Although Cl incorporation engineering has been widely used in PSCs, the characteristics of the chloride–iodide alloying structure in mixed-halide perovskites and its influence on the optoelectronic and morphological properties have been issues of a long-standing controversy [14]. This is why the role of Cl in PSCs is still under discussion today. In Figure 1a, a graphical comparison between iodide perovskite and chloride–iodide perovskite is depicted with the visual summary of the three main challenges of chloride-iodide PSC (in Figure 1b).

Currently, two critical issues for the commercial application of PSCs are efficiency and stability. Here, we present a systematic review of chloride–iodide PSCs concerning their efficiency and stability. From a review of the literature, we list various chloride–iodide PSCs. Then, we discuss different aspects of chloride–iodide PSCs from the list in Table 1. The advantages of Cl incorporation are discussed in detail concerning their optoelectronic and morphological characteristics. Then, we discuss different ways, such as composition, solvent, additive, deposition, annealing, and structural engineering, to overcome the issues related to Cl incorporation. We also suggest some future aspects of chloride–iodide PSCs. Note that while explaining different points, we present different chemical reactions with equations, mainly focusing on the products of the reactions hypothetically, and they are not stoichiometrically balanced on both sides.

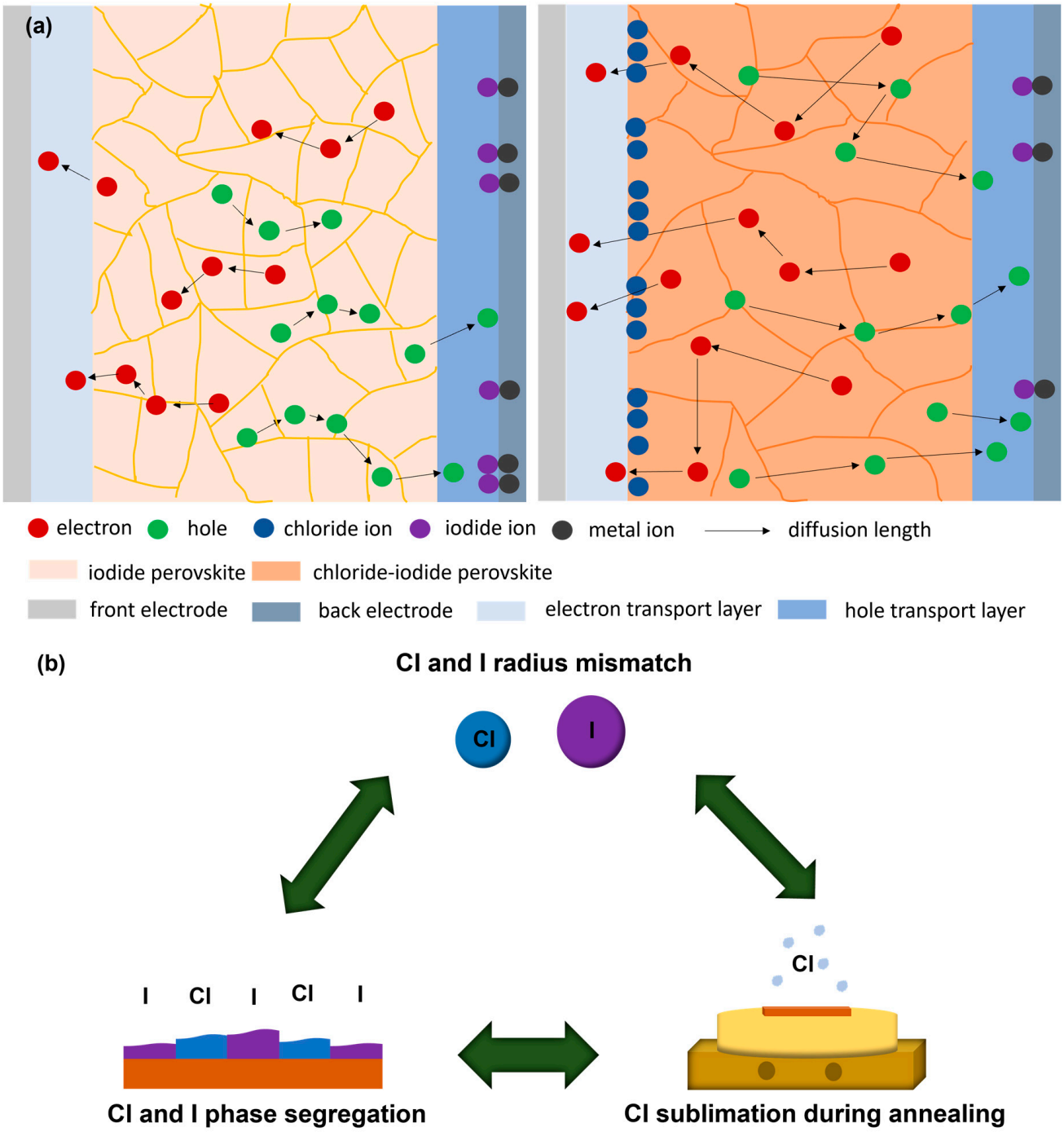

Figure 1. (**a**) Schematic representation of long diffusion length, long carrier lifetime, large grain size, more Cl^- ion migration, and less I^- ion migration in chloride–iodide perovskite compared to iodide perovskite. (**b**) Three major challenge of Chloride-iodide PSC: first is Cl and I radius mismatch, second is Cl and I phase segregation, and third is Cl sublimation during annealing.

Table 1. A table of chloride–iodide PSCs.

Solar Cell Architecture	Deposition Method	J_{sc} (mA/cm^2)	V_{oc} (V)	FF (%)	PCE (%)	Hysteresis (%)	Stability (Hours)	Cl (%)	Ref.
FTO/c-TiO_2/m-Al_2O_3/$MAPbI_2Cl$/Spiro-OMeTAD/Ag	One-step spin coat	15.40	1.13	45	10.90	-	-	33	[15]
FTO/TiO_2/$MAPbI_{3-x}Cl_x$/Spiro-OMeTAD/Ag	One-step spin coat	20.80	0.92	54	10.80	-	-	33	[16]
FTO/TiO_2/Al_2O_3/$MAPbI_{3-x}Cl_x$/Spiro-OMeTAD/Ag	One-step spin coat	18	1.02	67	12.30	-		40	[17]
FTO/TiO_2/$MAPbI_{3-x}Cl_x$/Spiro-OMeTAD/Ag	One-step spin coat	20.30	0.89	64	11.40	-	-	40	[18]
ITO/PEDOT:PSS/$MAPbI_{3-x}Cl_x$/PCBM/Al	One-step spin coat	18.50	0.87	72	11.50	-	-	40	[19]
ITO/PEDOT:PSS/$MAPbI_{3-x}Cl_x$/PCBM-C_{60}/Ag	One-step spin coat	18.30	0.91	70	11.65	-	-	25	[20]
FTO/TiO_2/$MAPbI_{3-x}Cl_x$/Spiro-OMeTAD/Au	Spin coat, dip coat	22.58	0.91	51	10.49	-	-	-	[21]
FTO/c-TiO_2/m-TiO_2/$MAPbI_2Cl$/Spiro-OMeTAD/Au	Spin coat, dip coat	19.91	1.09	65	14.15	-	-	-	[22]
FTO/TiO_2/$MAPbI_{3-x}Cl_x$/Spiro-OMeTAD/Au	Spin coat, dip coat	22.90	0.98	69	15.41	-	-	-	[23]
ITO/PEDOT:PSS/$MAPbI_{3-x}Cl_x$/PCBM/C_{60}/BCP/Ca-Al	Spin coat, drop coat	20.71	0.97	79	16.01	-	-	-	[24]
ITO/PEDOT:PSS/$MAPbI_{3-x}Cl_x$/PCBM/Ca-Al	Thermal evaporation, dip coat	19.58	0.99	78	15.12	-	720	-	[25]
FTO/c-TiO_2/$MAPbI_{3-x}Cl_x$/Spiro-OMeTAD/Ag	Vapor coat	21.50	1.07	67	15.40	-	-	33	[26]
FTO/TiO_2 $MAPbI_{3-x}Cl_x$/Spiro-OMeTAD/Ag	Spin coat, vapor coat	21.94	1.01	62	13.76	-	1152	-	[27]
FTO/c-TiO2/m-TiO2/$MAPbI_{3-x}Cl_x$/Spiro-OMeTAD/Au	One-step spin coat	21.35	0.97	68	14.05	-	-	25	[28]
ITO/TiO_2/$MAPbI_{3-x}Cl_x$/Spiro-OMetAD/Au	Spin coat, dip coat	21.45	1.08	77.57	17.91	-	-	-	[29]
FTO/c-TiO_2/$MAPbI_{3-x}Cl_x$/Spiro-OMeTAD/Au	One-step spin coat	21.50	1.04	76	16.90	-	-	40	[30]
ITO/TiO_x/$MAPbI_{3-x}Cl_x$/PTB7/Au	One-step spin coat	22.94	0.98	70	15.90	-	-	40	[31]
FTO/NiO_x/$MAPbI_{3-x}Cl_x$/PCBM-PEI/Ag	One-step spin coat	21.20	1.08	79.20	18.20	0.00	1500	-	[32]

Table 1. *Cont.*

Solar Cell Architecture	Deposition Method	J_{sc} (mA/cm^2)	V_{oc} (V)	FF (%)	PCE (%)	Hysteresis (%)	Stability (Hours)	Cl (%)	Ref.
FTO/c-TiO_x/$FAPbI_{3-x}Cl_x$/Spiro-OMeTAD/Au	One-step spin coat	22.30	1.01	77.40	17.40	-	-	7	[33]
ITO/PEDOT:PSS/$MAPbI_{3-x}Cl_x$/PCBM/BCP/Ag	One-step spin coat	20.78	0.99	73	15.02	-	-	-	[34]
ITO/PEDOT:PSS/$MAPbI_{3-x}Cl_x$/PCBM/Ag	One-step spin coat	20.60	0.98	77	15.70	-	-	25	[35]
ITO/CuO_x/$MAPbI_{3-x}Cl_x$/PCBM/C_{60}/BCP/Ag	One-step spin coat	22.50	1.11	75.80	19	-	-	10	[36]
FTO/c-TiO_2/$MAPbI_{3-x}Cl_x$/Spiro-OMeTAD/Au	One-step spin coat	22	0.10	72	16.10	-	-	40	[13]
ITO/NiO_x/$MAPbI_{3-x}Cl_x$/$PC_{61}BM$/AZO/Ag	Two-step spin coat	20.33	1.08	69	15.15	-	-	-	[37]
ITO/PEDOT:PSS/$MAPbI_{3-x}Cl_x$/RhB101/LiF/Ag	One-step spin coat	20.11	1.11	80.60	18	-	-	-	[38]
ITO/PEDOT:PSS/$MAPbI_{3-x}Cl_x$/PCBM/PEIE/Al	One-step spin coat	20.51	0.94	75	14.46	0.00	-	-	[39]
ITO/PEDOT:PSS/$MAPbI_{3-x}Cl_x$/CdSe-PCBM/LiF-Ag	One-step spin coat	20.96	0.90	73.16	13.73	-	-	67	[40]
ITO/PEDOT:PSS/$MAPbI_{3-x}Cl_x$/PCBM/Al	One-step spin coat	19.76	1.01	68	13.57	-	-	33	[41]
ITO/PEDOT:PSS/$MAPbI_{3-x}Cl_x$/ETL/PEI/Ag	One-step spin coat	18.88	1.01	76	14.52	-	-	-	[42]
ITO/PEDOT:PSS/$MAPbI_{3-x}Cl_x$/PCBM/PEI/Ag	One-step spin coat	20.20	1.08	79	17.2	-	-	-	[43]
FTO/PEDOT:PSS/$MAPbI_{3-x}Cl_x$/PCBM/Ag	One-step spin coat	22.59	0.97	62.61	13.72	-	-	33	[44]
FTO/TiO_2/$MAPbI_{3-x}Cl_x$/Spiro-OMeTAD/Au	Two-step spin coat	20.56	1.10	77.10	17.56	-	-	-	[45]
FTO/m-TiO_2/$MAPbI_{3-x}Cl_x$/Spiro-OMeTAD/Au	One-step spin coat	20.10	1	41	13.07	-	-	40	[46]
ITO/NiO_x/$MAPbI_{3-x}Cl_x$/$PC_{61}BM$/BCP/Ag	One-step spin coat	21.70	1.06	75	18.70	-	-	-	[47]
ITO/PEDOT:PSS/$MAPbI_{3-x}Cl_x$/PCBM/Ca-Al	One-step spin coat	20.39	0.95	80.30	15.55	0.00	-	40	[48]
ITO/PEDOT:PSS/$MAPbI_{3-x}Cl_x$/PCBM/Bphen/Ag	One-step spin coat	20.19	0.95	73	14.02	-	-	40	[49]
FTO/TiO_2/$MAPbI_{3-x}Cl_x$/Spiro-OMeTAD/Au	One-step spin coat	19.70	0.88	65	11.30	-	-	40	[50]
FTO/c-TiO2/$PC_{61}BM$/$MAPbI_{3-x}Cl_x$/Spiro-OMeTAD/Au	Spin coat, dip coat	23.77	1.09	74.86	19.49	-	-	-	[51]

Table 1. *Cont.*

Solar Cell Architecture	Deposition Method	J_{sc} (mA/cm^2)	V_{oc} (V)	FF (%)	PCE (%)	Hysteresis (%)	Stability (Hours)	Cl (%)	Ref.
FTO/c-TiO_2/$PC_{61}BM$/$MAPbI_{3-x}Cl_x$/Spiro-OMeTAD/Au	One-step spin coat	23.90	1.05	76	18.90	-	-	-	[52]
FTO/TiO_2/$PC_{61}BM$/$MAPbI_{3-x}Cl_x$/Spiro-OMeTAD/Au	Spin coat, dip coat	21.53	1.04	75.9	17	-	-	-	[53]
ITO/P3CT-Rb/$MAPbI_{3-x}Cl_x$/C_{60}/BCP/Ag	One-step spin coat	21.67	1.14	82.78	20.52	-	-	-	[54]
FTO/c-TiO_2/$MAPbI_{3-x}Cl_x$/Spiro-OMeTAD/Au	Vapor coat, spin coat	23.62	1.05	76.80	19.10	-	-	-	[55]
ITO/P3CT-N/$MAPbI_{3-x}Cl_x$/PCBM/BCP/Ag	One-step spin coat	22.10	1.12	81.97	20.36	1.47	10	-	[56]
FTO/c-TiO_2/$MAPbI_{3-x}Cl_x$/Spiro-OMeTAD/Ag	Two-step spin coat	25.86	1.12	59	17	-	-	10	[57]
FTO/c-TiO_2/$MAPbI_{3-x}Cl_x$/Spiro-OMeTAD/Ag	Three-step CVD	20.64	0.94	56.20	10.87	-	-	-	[58]
ITO/CNT-TiO_2/$MAPbI_{3-x}Cl_x$/CNT-P3HT/MoO_3-Ag	One-step spin coat	23.52	0.86	71	14.37	-	-	40	[59]
FTO/TiO_2/$MAPbI_{3-x}Cl_x$/PTAA/Au	One-step spin coat	22.10	1.11	77	19.10	0.00	-	40	[60]
FTO/c-TiO_2/$MAPbI_{3-x}Cl_x$/Spiro-OMeTAD/MoO_x-Au	One-step spin coat	23	1.06	72.10	17.50	-	-	40	[61]
ITO/DFBT-PMTP/$MAPbI_{3-x}Cl_x$/C_{60}/BCP/Ag	One-step spin coat	22.15	1.17	82.28	21.23	-	-	-	[62]

2. Advantages of Chloride–Iodide PSCs

Chloride–iodide perovskite has attracted significant attention due to the apparent performance enhancement obtained by using Cl doping. However, there are controversial arguments on the Cl function and its mechanism. The photovoltaic performance of PSCs depends on the perovskite film's optoelectronic and morphological properties. There are two distinct hypotheses about how the presence of Cl in perovskite improves these properties. The first explanation is related to optoelectronic properties. It is well established that Cl incorporation ensures improved optoelectronic properties, such as a long carrier diffusion length and lifetime. Specifically, other optical effects, such as absorption, photogeneration, etc., are not apparent yet [63]. Cl also has a significant impact on the electrical properties of perovskite. The electrical properties of perovskite are significantly enhanced by Cl doping. Doping passivates interfaces or grain boundaries and results in band bending at the interfaces. The second explanation is related to morphological properties. The presence of Cl improves crystalline features and film formation and leads to larger crystalline domains. Several recent papers offer optoelectrical and morphological explanations for the improvements observed in chloride–iodide perovskite [64]. In the following sections, we discuss the effects of Cl on the optoelectrical and morphological properties of chloride–iodide perovskite films and the efficiency and stability of related PSCs.

2.1. Effects on Optoelectronic Properties

Chloride–iodide perovskites show excellent optoelectronic properties and better photovoltaic performance than iodide perovskites, such as efficient charge carrier extraction at adjacent heterojunctions and transport within the bulk perovskite.

Cl usually preferentially localizes to the heterojunction interface in elemental form or as residual amorphous $PbCl_2$. Elemental Cl effectively passivates defects at the interface and facilitates band bending at the interface, while $PbCl_2$ hinders efficient charge extraction, as it is insulating [51,65]. Using angle-resolved X-ray photoelectron spectroscopy, Colella et al. [66] observed that Cl aggregates at the perovskite/TiO_2 interface. Unger et al. [67] also found Cl at both the grain boundaries and the interface from X-ray fluorescence measurements. Using steady-state and time-resolved photoluminescence, as well as electrochemical impedance spectra, Pham et al. [52] observed that adding 2.5% $PbCl_2$ increases the charge carrier lifetime and recombination resistance, while the photoluminescence peak drops noticeably in the presence of the charge transport layer with chloride–iodide perovskite due to efficient charge extraction. The performance of a related PSC, as reported by Pham et al. [52], is enhanced from an average PCE of 16.5% to 18.1% with a significantly improved fill factor (from 0.69 to 0.76). The dramatic improvement is due to the effective interfacial charge collection within the adjacent heterojunction. Cl is thus proposed to act as a dopant and surface passivator in the perovskite film.

Cl incorporation also facilitates charge carrier transport within the bulk perovskite crystals. At the same time, it enhances electron diffusion and collection in the film due to reduced crystalline defects. Chen et al. [29] found two-times longer charge carrier lifetime in chloride–iodide perovskite than in iodide perovskite films. Again, they used the capacitance–voltage technique to find defect activation energies of 21.6 and 74.4 meV for chloride–iodide and iodide films, respectively. This indicates that Cl incorporation results in shallower defects along the film. These superficial defects are the result of fewer crystalline defects in the chloride–iodide perovskite film. Crystalline defects generate deep trap states in the bandgap of perovskite and reduce the number of collectible electrons. In this way, Cl incorporation improves the PCE of PSCs.

2.2. Effect on Crystalline and Morphological Properties

The photovoltaic performance of PSCs highly depends on the film's crystallinity and morphology [14]. Crystalline factors in the context of large domain sizes and compact structures such as cubic ones are standard for better photovoltaic performance. Morphological aspects in the context of surface coverage and film conformity are well known to affect the photovoltaic performance of PSCs [68].

Better crystalline features, such as oriented crystalline growth, larger atomic order, and dense coordination, are observed with chloride–iodide perovskite films. Lee et al. [15] observed X-ray diffraction peaks at angles of 14.20°, 28.58°, and 43.27° for the chloride–iodide film, which correspond to the (110), (220), and (330) planes. The results confirm a tetragonal perovskite structure with lattice parameters a = 8.825 Å, b = 8.835 Å, and c = 11.24 Å, which are similar to those of the iodide-based film. They noticed narrow diffraction peaks, indicating that the film had a long-range crystalline domain. It was also found that a small amount of Cl can substitute for I in the PbI_6 inorganic lattice, which leads to a phase transition from the tetragonal to the cubic phase [69]. Introducing Cl into the perovskite lattice increases the Goldsmith tolerance factor's value and the photoactive phase's stability [70]. McLeod et al. [71] observed that a chloride–iodide film sample made with excess $PbCl_2$ had the highest Pb-I coordination, which was found to be six by fitting the Pb L3-edge extended X-ray absorption spectra with a three-shell model. Therefore, Cl contributes to a compact crystalline structure. The stronger electronegativity of Cl vs. I and the associated more rigid bonds formed with Pb^{2+} ions help restrain lattice distortions.

Chloride–iodide perovskite also manifests compact films with good surface coverage. Xu et al. [72] found that a small amount of Cl doping (less than 5%) significantly increased the perovskite grain size, and the related PSC exhibited up to 17.44% PCE. When imaging the chloride–iodide film, the reflection and diffraction micrographs showed an increase in the surface coverage of oriented grains from 2.5% (in the case of iodide film) to 5.5% (in the case of chloride–iodide film (Cl doping 7%)) [73].

3. Engineering of Chloride–Iodide PSCs

From the above discussion, it is evident that adding Cl to I-based PSCs results in outstanding photovoltaic performance due to better optoelectrical, crystalline, and morphological properties [74]. Despite these advantages, there are various obstacles to incorporating Cl into the perovskite system. The most surprising fact is that the Cl percentage calculated from the precursor solution is not detectable in the final perovskite film. There are three acceptable hypotheses to explain this phenomenon. The first is the radius difference between Cl^- and I^- ions. Second, Cl affects the nucleation dynamics of perovskite, and an intermediate phase forms during growth. As a result, chloride–iodide perovskite is prone to phase segregation. The third one proposes that Cl disappears upon thermal annealing [75]. Here, we discuss the strategies employed in various studies in the literature to solve these issues, such as composition, solvent, additive, deposition, annealing, and structural engineering.

3.1. Precursor Composition Engineering

There is a long-standing debate that the exact concentration of Cl in the final film does not reproduce the stoichiometry of the precursor solution. Cl incorporation into I-based perovskite film is only possible at relatively low concentrations [76]. Precursor compositions determine the Cl contents in chloride–iodide perovskite and the photovoltaic performance. Therefore, it is necessary to investigate the effect of components' molar ratio in precursor solutions such as MAI, MACl, PbI_2, and $PbCl_2$.

To investigate the effect of components' molar ratio in precursor solutions, Colella et al. [77] developed chloride–iodide films using two different molar ratios of precursor solution components. The first was MAI:$PbCl_2$ (3:1), and the second was MACl:PbI_2 (1:1). Diffraction patterns for both samples showed highly oriented crystalline films. At the same time, energy-dispersive X-ray spectroscopy measurements cannot detect reliable values of the Cl concentration. The first and second films manifest 6.15% and 3.85% PCEs, respectively. Therefore, the MAI:$PbCl_2$ (3:1) precursor composition is preferable to MACl:PbI_2 (1:1). With the MAI:$PbCl_2$ (3:1) precursor composition, due to a higher quantity of MAI, $MAPbCl_3$ forms. For example, Yantara et al. [78] developed chloride–iodide perovskite films with the MAI:$PbCl_2$ (3:1) molar ratio and observed that the film sample undergoes a color change before the film turns completely dark brown. The chloride–iodide film undergoes a color evolution from brown to light brown to dark brown. They hypothesized the following reaction for the initial brown film:

$$MAI + PbCl_2 \rightarrow MAPbI_3 + MAPbCl_3 + MAI + MACl + PbI_2 \quad (1)$$

They also observed that after annealing for a while, the brown film (see Figure 2a) first turns light brown (see Figure 2b). The formation of a higher quantity of $MAPbCl_3$ is the reason for the color change. The bandgap of $MAPbCl_3$ is higher than that of $MAPbI_3$ and light brown. $MAPbI_3$ dissociates into MAI and PbI_2 and leaves behind MACl and $MAPbCl_3$. At the same time, MACl also reacts with $MAPbI_3$ and forms $MAPbCl_3$. Due to the excess amount of $MAPbCl_3$, the film seems light brown. This phenomenon arises due to unreacted excess MAI in the system. The following reaction represents the intersubstitution of Cl and I in the process of $MAPbCl_3$ generation.

$$MAPbI_3 + MACl \leftrightarrow MAI + MAPbCl_3 \quad (2)$$

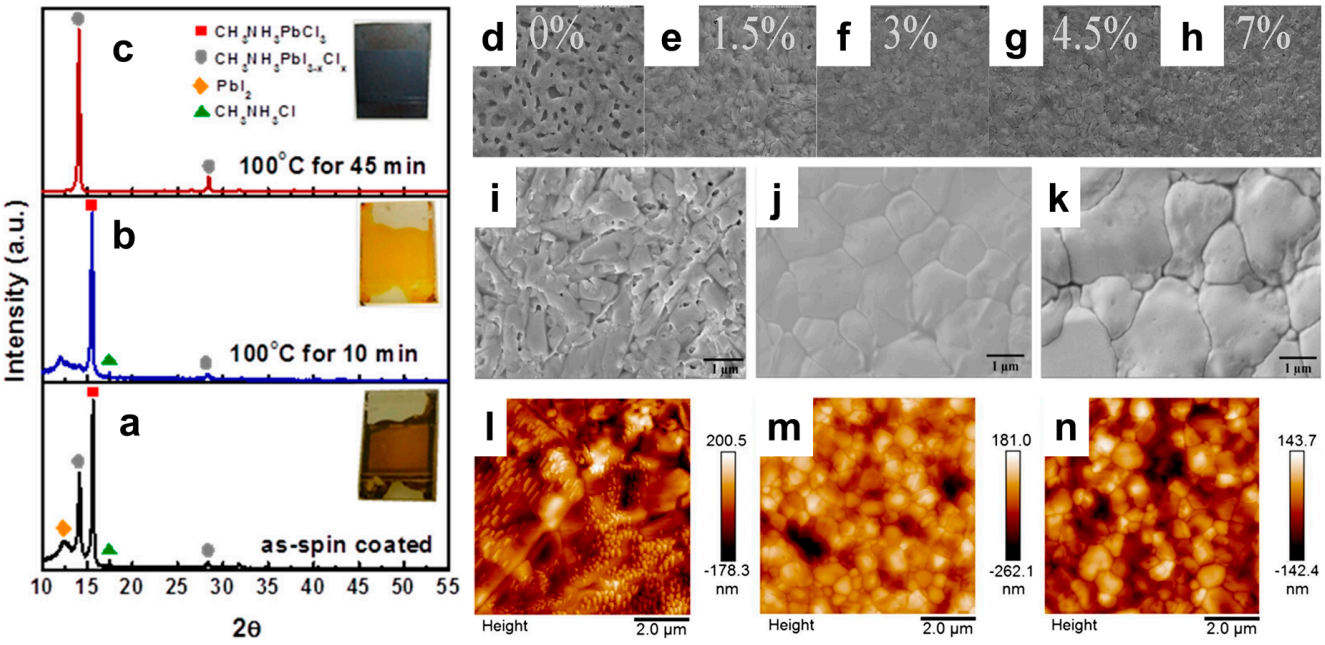

Figure 2. Color evolution of the chloride–iodide perovskite film with annealing time and the corresponding X-ray diffraction patterns. The insets show the optical images of the films. (**a**) As-spin-coated. (**b**) After 10 min. (**c**) After 45 min [78]. Scanning electron microscopy images of chloride–iodide perovskite films deposited with various amounts of extra $PbCl_2$: (**d**) 0%, (**e**) 1.5%, (**f**) 3%, (**g**) 4.5%, (**h**) 7% [13]. Scanning electron microscopy images of chloride–iodide perovskite films obtained with different ratios of precursor solutions: (**i**) 3:1 (MAI:$PbCl_2$), (**j**) 4:1:1 (MAI:PbI_2:$PbCl_2$), (**k**) 1:1:1 (MAI:MACl:PbI_2). Atomic force microscopy images of chloride–iodide perovskite films obtained with different precursor solutions: (**l**) 3:1 (MAI:$PbCl_2$), (**m**) 4:1:1 (MAI:PbI_2:$PbCl_2$), (**n**) 1:1:1 (MAI:MACl:PbI_2) [79].

After further annealing, the light-brown film (see Figure 2b) transforms into dark brown (see Figure 2c), indicating the presence of a higher quantity of $MAPbI_3$ or mixed chloride–iodide perovskite. The possible chemical reaction is demonstrated as follows:

$$MAPbCl_3 + MAI + PbI_2 \rightarrow MAPbI_3/MAPbI_{3-x}Cl_x + MACl \quad (3)$$

In this context, it is necessary to reduce the extra MAI in the system because extra MAI helps to produce $MAPbCl_3$, which is undesirable and degrades the PCE. $MAPbCl_3$ has a low boiling temperature, and during annealing, $MAPbCl_3$ decomposes into MACl and $PbCl_2$. MACl is highly volatile and escapes from the film during annealing. As a result, Cl vacancies and undesirable defects are created. To mitigate this issue, Huang et al. [13] deliberately introduced excess $PbCl_2$ in the chloride–iodide perovskite precursor. They varied the molar ratio of MAI to $PbCl_2$ as 3:1, 3:1.015, 3:1.03, 3:1.045, and 3:1.07. The excess $PbCl_2$ also results in dense and uniform films consisting of large micron-sized grains, as shown in the scanning electron microscopy images in Figure 2d–h. In another study, Zhang et al. [50] fabricated chloride–iodide PSCs using precursor solutions containing MAI and $PbCl_2$ with molar ratios of 1:1, 3:1.05, 3:1.10, and 3:1.15, respectively. The PSC with a mole ratio of 3:1.05 presented the highest PCE, which means that a 10% Cl atomic concentration is optimal.

Now, from the above discussion, it is understood that excess MAI can form a $MAPbCl_3$ phase. In contrast, it is believed that a much higher concentration of Cl might reduce the PCE. Therefore, it is necessary to investigate the influence of different MA^+ and Cl^- ion concentrations' effects in more detail. At the same time, the MA^+ and Cl^- ion sources from different precursors should be investigated. For this purpose, Tombe et al. [79]

studied a set of various precursor formulations to understand the correlations between the MA^+ and Cl^- ionic composition and the resulting PSC performance. Three precursor solutions with different ratios of MAI, MACl, PbI_2, and $PbCl_2$, such as 3:1 (MAI:$PbCl_2$), 4:1:1 (MAI:PbI_2:$PbCl_2$), and 1:1:1 (MAI:MACl:PbI_2), were used. The corresponding film morphology is shown in scanning electron microscopy images (see Figure 2i–k) and atomic force microscopy (see Figure 2l–n) images. PSCs made from 4:1:1 (MAI:PbI_2:$PbCl_2$) and 1:1:1 (MAI:MACl:PbI_2) combinations showed nearly identical, good PCEs, which were better than the 3:1 (MAI:$PbCl_2$) combination.

The PSC obtained from the 1:1:1 (MAI:MACl:PbI_2) formulation showed good stability in a nitrogen environment. The composition of ions in the two 4:1:1 (MAI:PbI_2:$PbCl_2$) and 1:1:1 (MAI:MACl:PbI_2) precursor formulations were identical (MA^+:Pb^{2+}:I^-Cl^- = 2:1:3:1), while the composition of ions in the 3:1 (MAI:$PbCl_2$) precursor formulation was (MA^+:Pb^{2+}:I^-:Cl^- = 3:1:3:2). In the last case of the 3:1 (MAI:$PbCl_2$) precursor formulation, there were excess amounts of MA^+ and Cl^- ions, especially the content of Cl^- ions, which was twice as high. The above results indicate that a higher concentration of extra Cl^- ions degrade the PCE. A small excess Cl^- ions reduces the possibility of $MAPbCl_3$ formation. Therefore, the overall ionic composition in the precursor solution is crucial for chloride–iodide perovskite formation and PCE. Here, the source of these ions, however, appears to be irrelevant.

3.2. Additive Addition Engineering

Additives play an essential role in perovskite crystal growth and the performance of PSCs [80,81]. Additive addition is an alternative way to improve the photovoltaic performance and stability of chloride–iodide PSCs [82]. Here, we will discuss the additive's role in incorporating Cl into chloride–iodide perovskite. The previous section summarizes results showing that excess Cl^- ions degrade the PCE, while a small excess of Cl^- ions offers better PCE. Generally, additives are added to the perovskite precursor solution in meager amounts. Thus, there is a low probability of excess Cl^- ions in the perovskite film.

One of the possible ways to add Cl to iodide perovskite is to add familiar sources of Cl, such as MACl (methyl ammonium chloride), FACl (formamidinium chloride), etc., which are also the basic constituent precursors of chloride–iodide perovskites [33,83]. When these precursors are added to the iodide-based perovskite precursor solution in excess amounts, it helps to yield chloride–iodide perovskite. At the same time, there is a possibility of generating mixed individual phases in the perovskite film. We have found in the previous section that extra MA^+ or FA^+ ions produce $MAPbCl_3$ or $FAPbCl_3$. Thus, there is a possibility of the creation of an alloy of pure halide perovskites, such as $MAPbI_3$ and $MAPbCl_3$ or $FAPbI_3$ and $FAPbCl_3$. $MAPbCl_3$ possesses low formation energy and a low boiling temperature. $MAPbCl_3$ decomposes into MACl and $PbCl_2$. Again, during the annealing process at more than 100 °C, MACl leaves the perovskite film, resulting in the loss of Cl. It is known to all that annealing is an indispensable and crucial part of the formation of high-quality perovskite crystals. The common fabrication method involves spin coating the precursor solution onto the substrate. After that, usually, complete crystallization is obtained by annealing. Annealing is used to evaporate the organic polar solvent from the perovskite film, which helps to control the morphological and structural properties of the films. Annealing also eliminates residual stresses and internal defects within the film [84]. Usually, if annealing is not performed with a perovskite film, it requires the addition of specific reagents, such as guanidine iodide, to the precursor solution [85]. The Cl vacancies ultimately produce undesirable pinholes or cracks in the film. These issues make it challenging to dope Cl into the iodide-based perovskite matrix.

In this respect, researchers have used alternative sources of additives to incorporate Cl into the iodide-based perovskite system. For example, Wu et al. [56] selected Cl-FACl as an additive to stabilize chloride–iodide perovskite and thus restrain the removal of Cl and avoid undesirable defects in the film. They describe their postulated reaction process as follows:

$$\text{Cl-FACl} + \text{MAI} + \text{PbI}_2 \rightarrow \text{Cl-FAI} + \text{MACl} + \text{PbCl}_2 \quad (4)$$

$$\text{MAI} + \text{MACl} + \text{PbI}_2 + \text{PbCl}_2 \rightarrow \text{MAPbI}_{3-x}\text{Cl}_x + \text{MACl} \quad (5)$$

$$\text{Cl-FAI} + \text{MACl} \rightarrow \text{Cl-FACl} + \text{MAI} \quad (6)$$

In the first step of the reaction, MACl and $PbCl_2$ are formed. The chloride ion has stronger electronegativity than the iodide ion. Thus, iodide ions in MAI and PbI_2 exchange with chloride ions to produce MACl and $PbCl_2$. In the second step, during chloride–iodide perovskite film formation, the Cl^- ions further exchange with I^- ions and transform into a chloride–iodide perovskite film. Furthermore, the Cl-FA^+ ions capture the Cl^- ions and restrain the removal of MACl during annealing, as MACl is volatile. In this way, the film quality improves, and defects are reduced after the introduction of Cl-FACl. Time-resolved photoluminescence of this sample shows a longer decay time, thus offering a more stable device. The PSC delivers efficiency of up to 20.36% with negligible hysteresis. The device also presents more than 94% of its initial performance after testing for 600 min.

Another interesting suggestion is that water could be an effective additive for chloride–iodide perovskite. Water behaves like a highly coordinated polar aprotic solvent and can be positively used as an additive. The idea of using water as an additive comes from the evidence that large-grain perovskite films with a lower defect density can be obtained by controlling the amount of humidity or moisture. Humidity or moisture represents the amount of water in the atmosphere. On the other hand, humidity or moisture decomposes perovskite into its compositional elements. Thus, it seems that water is harmful to perovskite films. Here, we see that water plays a dual role. Perovskite film's crystallinity increases when an optimal amount of water is added but decomposes when an extra amount of water is added [86]. Therefore, it is interesting to investigate the role of water as an additive in chloride–iodide perovskite. To clarify the mysterious role of water, Li et al. [30] fabricated chloride–iodide film through an aquointermediate process. Here, water works as an additive. The film grows highly oriented along the (110) crystalline direction. Its diffraction intensity ratio of (110)/(310) is nearly two orders of magnitude higher than that of the film prepared traditionally, as shown in Figure 3a. During the formation process of the film prepared in the traditional way, three species are found, namely, $MAPbI_{3-x}Cl_x$, $MAPbI_3$, and $MAPbCl_3$, as described below:

$$\text{MAI} + \text{PbCl}_2 \rightarrow \text{MAI} + \text{MACl} + \text{PbI}_2 \rightarrow \text{MAPbI}_{3-x}\text{Cl}_x + \text{MAPbI}_3 + \text{MAPbCl}_3 \quad (7)$$

whereas only $MAPbI_{3-x}Cl_x$ is obtained through the aquointermediate process, as described below.

$$\text{MAPbI}_3 + \text{MAPbCl}_3 + \text{H}_2\text{O} \rightarrow \text{MAPbI}_{3-x}\text{Cl}_x\cdot\text{H}_2\text{O} \rightarrow \text{MAPbI}_{3-x}\text{Cl}_x \quad (8)$$

In the aquointermediate process, the chloride–iodide perovskite solution turns into powder through hydrolysis with 50% moisture. The powder is then dissolved into dimethylformamide and spin-coated to form the film. The simple halide exchange (Cl → I) process forms a high-quality film during annealing. The aquointermediate fabrication process is depicted in Figure 3b. The related PSC manifests a PCE of 16.9% with better thermal stability.

3.3. Solvent Composition Engineering

In perovskite film preparation, the solvent plays a critical role. Solvents not only play the role of dissolving the solutes but also determine the crystallization route. The chemical kinetics of perovskite precursors influence the microstructural properties [87]. Crystallization depends on the capacity of the precursor components to interact with each other in the solvent. Different solvents have different evaporation rates and solubilize the precursors in various ways due to their different chemical kinetics. Different solvents and solvent additives modify the structural uniformity and crystallinity of the perovskite film [88]. Here, we will discuss the solvent's role in incorporating Cl into I-based perovskites.

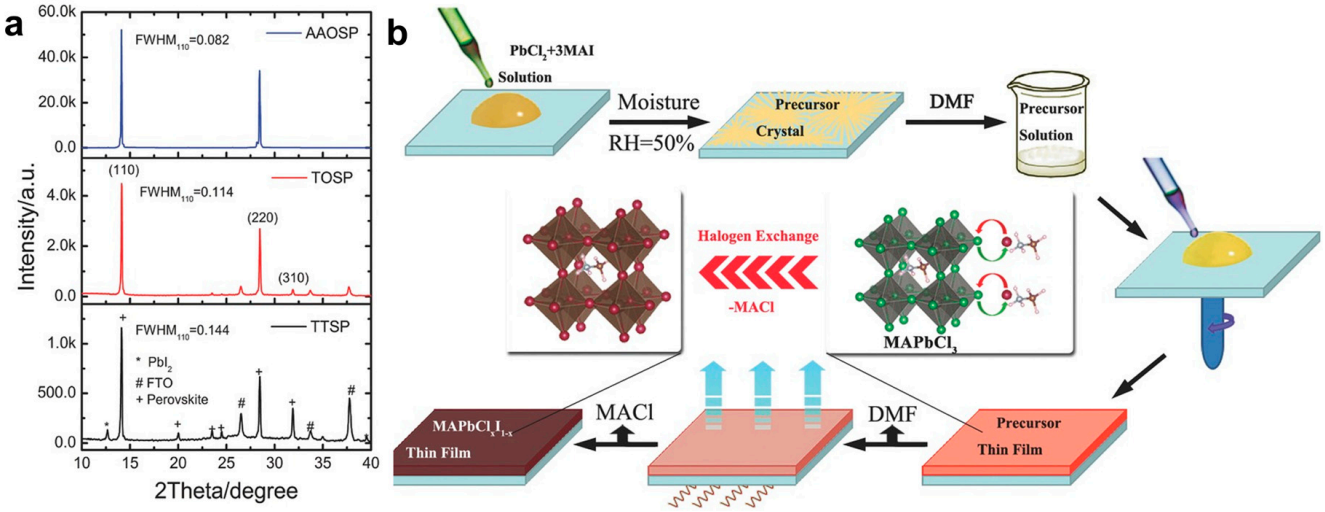

Figure 3. (**a**) X-ray diffraction pattern of chloride–iodide perovskite films prepared by traditional and aquointermediate processes. (**b**) Schematic view of the aquointermediate process for the fabrication of chloride–iodide perovskite film [30].

From the previous sections, we find that the most convenient process of preparing chloride–iodide perovskite films is to use a 3:1 molar mixture of MAI:$PbCl_2$ in a solution. In this process, there is a problem of excess unreacted MAI, as about three times more MAI than $PbCl_2$ is used. The excess MAI produces $MAPbCl_3$. The melting temperature and formation energy of $MAPbCl_3$ are low. Therefore, during annealing, $MAPbCl_3$ decomposes into MACl, and MACl leaves the film. This phenomenon produces various defects in the film, ultimately losing Cl. The chemical reaction in this process can be represented as follows:

$$MAI + PbCl_2 \leftrightarrow MAPbI_{3-x}Cl_x + MAI + MACl \quad (9)$$

Mehdi et al. [89] explored the PCE of chloride–iodide PSCs with different volumes of dimethylformamide (DMF) and dimethyl sulfoxide (DMSO) as solvents. Their observations were based on four different solvent volume ratios of DMF:DMSO: 100:0, 80:20, 50:50, and 0:100. The highest PCE was obtained for the solar cell made in pure DMF. In X-ray diffraction spectra, they observed higher peak intensity in 100% DMF samples than in samples made from different volumes of DMSO. This result indicates the complete crystallization of the perovskite film. This result also shows that the chemical kinetics of the precursor elements of chloride–iodide perovskite are more suitable in DMF than in DMSO. The samples from 100% DMF also provided the lowest photoluminescence intensity, indicating the low charge carrier recombination, and the highest separation efficiency with the fastest migration process. In contrast, the samples with different volumes of DMSO showed the highest photoluminescence intensity. The results indicate a high number of surface defects due to the poor infiltration of the perovskite precursors, leading to high charge recombination. Fewer defects mean fewer Cl vacancies, less sublimation of MACl

during annealing, and ultimately less unreacted MAI. DMF has a lower viscosity than DMSO. Therefore, it can be assumed that the chemical kinetics of different precursors of chloride–iodide perovskite are more favorable with less viscous solvents.

3.4. Deposition Method Engineering

Morphological control is a bottleneck in controlling state-of-the-art PSCs, especially mixed-halide perovskites. Some significant obstacles, including the generation of the alloying composition of $MAPbI_3$ and $MAPbCl_3$, the presence of unreacted MAI, and the sublimation of Cl, are crucial in the case of chloride–iodide perovskite. Cl vacancy defects are generated due to the sublimation of MACl. The film thickness is also related to the morphological properties of perovskite. Usually, a thicker perovskite film has fewer pinholes. Different deposition methods are used to overcome these obstacles. Here, we discuss various deposition methods of chloride–iodide films and the resulting PSC performance. Solution and evaporation process deposition methods are prevalent for chloride–iodide perovskite film deposition.

3.4.1. Solution Process Deposition

Solution process deposition is one of the main advantages of PSCs. This process not only is very cheap but also requires simple equipment and a low temperature. The prevalent methods used for solution process deposition are spin coating, dip coating, slot-die coating, and spray coating. Spin and dip coating are for small-scale production, whereas slot-die and spray coating are for large-scale production.

Spin Coating

Perovskite film deposited by spin coating using a single solution is known as one-step spin coating. A mixture of metal halide and organohalide salts in a specific ratio is typically dissolved in a common solvent to make a single solution. Perovskite film deposition by spin coating in two steps, where two different solutions are deposited step by step, is known as two-step spin coating. Here, two different halide and organohalide salts at specific concentrations are typically dissolved in two other solvents.

1. One-Step Spin Coating

One-step spin coating is one of the simplest methods for depositing perovskite films. The morphology of the perovskite film, specifically the film coverage, is controlled with different spin speeds and spin times in one-step spin coating [18,19]. However, the formation of a compact chloride–iodide perovskite film is not feasible with one-step spin coating, as there are two halide elements. In one-step spin coating, there are more than two precursor salts in one single solution to deposit the chloride–iodide perovskite film. For example, Wang et al. [20] developed compact chloride–iodide perovskite films using one-step spin coating from mixed lead halide precursors. The single solution contained MAI, PbI_2, and $PbCl_2$ with a molar ratio of 4:1:1. The possible chemical reactions are described as follows:

$$MAI + PbI_2 \rightarrow MAPbI_3 \quad (10)$$

$$MAI + PbCl_2 \rightarrow MAPbI_{3-x}Cl_x + MAI + MACl \quad (11)$$

$$MAPbI_3 + MAI + PbCl_2 \rightarrow MAPbI_{3-x}Cl_x + MAI + MACl \quad (12)$$

PbI_2 is more reactive with MAI than $PbCl_2$. The formation of the chloride–iodide film may not be possible due to the difference in the reaction kinetics between MAI and PbI_2 or $PbCl_2$. The solubility of PbI_2 and $PbCl_2$ is low, even in dimethylformamide. Due to high MAI content, which is about four times that of PbI_2 or $PbCl_2$, there are two different phases: $MAPbI_3$ and $MAPbCl_3$. $MAPbCl_3$ has a low boiling point temperature and formation energy. During annealing, $MAPbCl_3$ decomposes into MACl and $PbCl_2$. MACl is too

volatile and escapes from the film, creating Cl vacancies. Cl vacancies significantly affect the PCE.

2. Two-Step Spin Coating

The chloride–iodide perovskite is made from a mixture of halogen salts (MAI, MACl, PbI_2, $PbCl_2$, etc.) in a common solvent in the one-step spin coating method. The solubilities of PbI_2 and $PbCl_2$ are low, even in dimethylformamide. Hence, two different solvents are used for different precursors in two-step spin coating. In two-step spin coating, a PbI_2 or $PbCl_2$ film is deposited in the first step, and the chloride–iodide film is formed from another MAI or MACl solution spin coating in the second step. Here, chloride–iodide perovskite film growth becomes more controllable because the nucleation and reaction rates can be independently manipulated [68]. Despite the above advantages of two-step spin coating compared to single-step spin coating, there are also some challenges in two-step spin coating.

The first challenge of two-step spin coating is the generation of the intermediate phase in the first step of two-step spin coating. According to Fan et al. [51], in the PbI_2 and $PbCl_2$ mixture solution, it is possible to generate a PbICl intermediate phase. The corresponding chemical reaction is given below.

$$PbI_2 + PbCl_2 \rightarrow PbICl \quad (13)$$

There is also the possibility of unreacted PbI_2. Therefore, in the second step of two-step spin coating, there can be two chemical reactions, as follows:

$$MAI + PbICl \rightarrow MAPbI_{3-x}Cl_x + PbCl_2 \quad (14)$$

$$MAI + PbI_2 \rightarrow MAPbI_3 \quad (15)$$

Thus, after the second step, there is excess $PbCl_2$ in the system. In addition, PbICl decomposes into PbI_2 and $PbCl_2$. This excess $PbCl_2$ ultimately produces $MAPbCl_3$ as follows:

$$MAI + PbCl_2 \rightarrow MAPbCl_3 + PbICl \quad (16)$$

$MAPbCl_3$ production is detrimental to perovskite films. Because the boiling temperature and formation energy of $MAPbCl_3$ are low, it is easy to transform $MAPbCl_3$ into MACl. MACl is volatile and can escape from the film during annealing. This phenomenon creates Cl vacancies in the film and degrades PCE. All the steps in two-step spin coating for the device fabrication process are depicted in Figure 4a. The PCE is 19.49%, and the corresponding J-V curve and external quantum efficiency with the integrated photocurrent are shown in Figure 4b,c, respectively.

The second challenge of two-step spin coating is the film's generation of two regions (chloride-rich and iodide-rich). Compositional heterogeneities or non-stoichiometric areas modify the formation energies of deep-lying defects [90]. For example, Ko et al. [45] spin-coated a mixture of PbI_2 and $PbCl_2$ solutions in dimethylformamide in the first step. Then, the MAI solution in isopropanol was spin-coated in the second step to form the chloride–iodide perovskite film. They observed strange interdiffusion in the film because, after the second step, due to the interdiffusion process, the lower section of the film lacks iodine, while the upper section becomes iodine-rich. According to their observations, there are two different regions in the film: Region I, which is iodide-rich and chloride-poor, and Region II, which is iodide-poor and chloride-rich. The chemical reactions in these two regions are given below.

Region I:

$$PbI_{3-x}Cl_x \text{ (intermediate phase)} + MAI \text{ (sufficient)} \rightarrow MAPbI_{3-x}Cl_x + MACl \quad (17)$$

Region II:

$$PbI_{3-x}Cl_x \text{ (intermediate phase)} + MAI \text{ (insufficient)} \rightarrow MAPbI_{3-x}Cl_x + PbI_2 + MACl \quad (18)$$

In Region I, ample MAI species exist. The available MAI helps to convert the unstable intermediate $PbI_{3-x}Cl_x$ phase into perfectly stoichiometric $MAPbI_{3-x}Cl_x$. At the same time, MACl can flow out from the surface. MAI diffuses from Region I to Region II very slowly. Region II is deficient in MAI. This deficiency disrupts the stoichiometric balance of chloride–iodide perovskite.

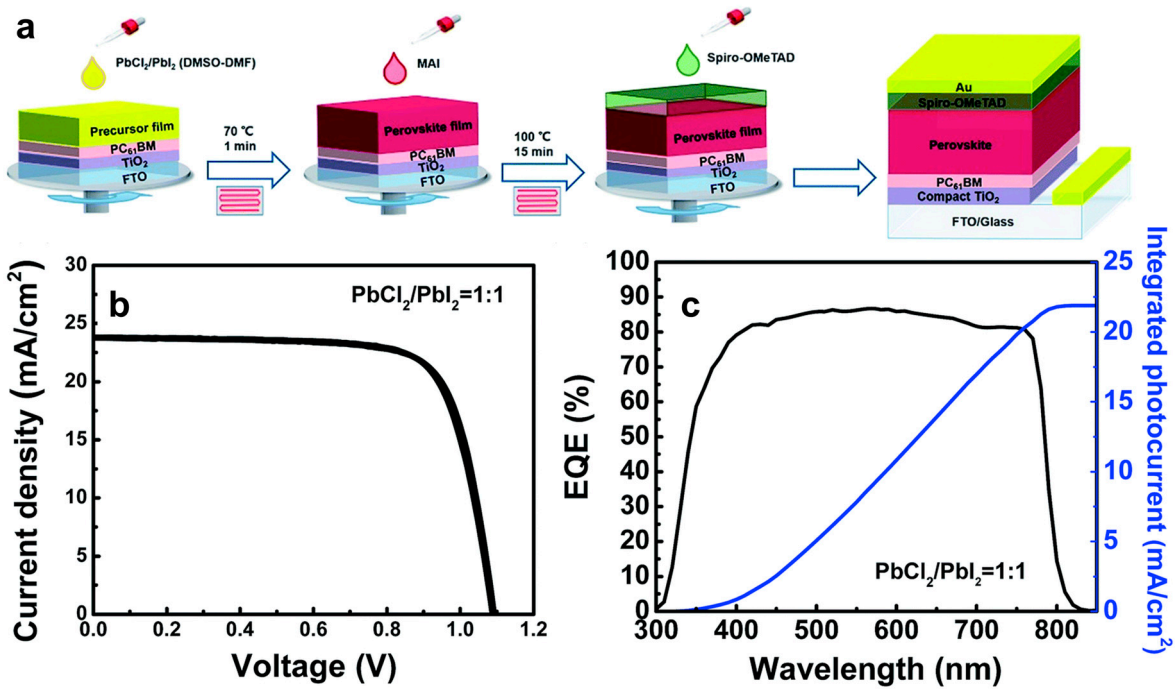

Figure 4. (**a**) Schematic illustration of the device fabrication process with two-step spin coating. (**b**) J-V curve with negligible hysteresis for the related device. (**c**) External quantum efficiency spectrum and integrated photocurrent of the related device [51].

Due to the low possibility of forming a stoichiometrically balanced chloride–iodide film in the two-step spin-coating process, the second step is altered by introducing dip coating. In spin coating, the interdiffusion of MAI might not happen properly due to the centrifugal force caused by rotation. In dip coating, PbI_2 or $PbCl_2$ or their mixed film is dipped vertically in MAI, MACl, or their hybrid solution, which may facilitate proper interdiffusion. For example, Jiang et al. [21] spin-coated PbI_2 onto the substrate and then dipped the film into a solution of MAI:MACl in isopropanol to form a complete chloride–iodide film. Figure 5a shows the dip-coating procedure. The reaction between PbI_2 and MACl occurs efficiently, facilitating the formation of the chloride–iodide film. This is evident from the surface and cross-sectional scanning electron microscopy images in Figure 5f,g,j. The resulting film is homogeneous and densely packed. Another PSC made with the same method by Docampo et al. [23] showed a PCE of 15.41%, where the spin-coated PbI_2 film was preheated before the film was dipped into a heated MAI:MACl solution. In another work, Dharani et al. [22] added only 10 mol% $PbCl_2$ with PbI_2 and spin-coated it onto a substrate to make the film. Then, they dip-coated in the MAI solution and obtained better perovskite morphology. Cao et al. [53] prepared a PSC similarly and obtained a PCE of 17%. In another work, Dong et al. [24] used multicycle solution-based

spin and dip coating. In this method, the PbI_2 film was spun onto the substrate and annealed. Then, the PbI_2 film was dipped in the MAI:MACl solution and annealed. This cycle continued until obtaining the film was thick enough. This multicycle interdiffusion results in substantial and well-oriented grains. The large grain size with reduced a grain boundary area contributes to a PCE of 18.9%.

Blade Coating and Slot-Die Coating

For fabricating lab-scale perovskite film, spin coating and dip coating are very popular methods. Spin coating and dip coating are not as favorable due to the difficulty of scaling up, so alternative thin-film coating methods such as blade coating and slot-die coating are much more popular. For the large-scale fabrication of PSCs, there are several challenges, such as poor interfacial contact between the perovskite layer and ETL/HTL; the amplification of bulk defects such as voids, pinholes, or impurities; and enhanced carrier recombination [91]. During large-size PSC fabrication, uncontrollable chemical kinetics during the transformation from $PbI_2/PbCl_2$ to perovskite is the key reason that macroscopic voids, pinholes, and contact defects occur. To remove these defects, a perovskite film of more than 1µm thickness needs to be fabricated. The primary problem is that the carrier diffusion length of $MAPbI_3$ is much less than 1µm and is not suitable for large-size PSCs. Fortunately, chloride–iodide perovskite has a carrier diffusion length of more than 1µm and can be used to produce large-size PSCs.

3.4.2. Evaporation Process Deposition

Vapor-phase deposition suggests a potential solution to the limits imposed by solution process deposition in incorporating Cl into chloride–iodide perovskite [92]. In solution process deposition, we have seen in the previous sections that there is a possibility of generating MACl as a byproduct. MACl is volatile and can escape from the final perovskite film during annealing. Thus, there is a possibility of Cl vacancy generation. Vapor process deposition does not need any post-annealing treatment and reduces the probability of Cl vacancy creation. Again, the solubility of $PbCl_2$ is very low in dimethylformamide, even lower than that of PbI_2. The poor solubility of PbI_2 or $PbCl_2$ generally leads to significant morphological variations in the chloride–iodide perovskite film in solution process deposition, and ultimately, unstable device performance occurs. One of the main drawbacks of solution process deposition is the presence of pinholes, resulting in direct contact between the absorbing layer and the charge transport layer. This incident leads to a shunting path, a possible reason for the lower PCE with the solution process. In the vapor-phase deposition process, better morphological features, such as large uniform films, large grain size, fewer pinholes, etc., can be obtained.

Vapor-phase deposition can be performed in two ways: the co-evaporation of individual precursor elements or the sequential evaporation of precursor elements. Ngqoloda et al. [58] fabricated chloride–iodide perovskite films through facile two-step and three-step sequential vapor-phase deposition. In two-step vapor-phase deposition, $PbCl_2$ and PbI_2 are deposited in the first step and converted to chloride–iodide perovskite in the second step. In three-step vapor-phase deposition, first $PbCl_2$ is deposited, followed by PbI_2, and chloride–iodide perovskite is formed in the third step. These deposition steps are shown schematically in Figure 6a, together with the conversion to chloride–iodide perovskite. It is seen in Figure 6b–d that more compact morphology is obtained with three-step compared to two-step vapor-phase deposition. Liu et al. [26] observed crystalline features on the length scale of hundreds of nanometers in scanning electron microscopy images from the vapor-phase-deposited chloride–iodide perovskite film. In contrast, crystalline features on a length scale of tens of micrometers were found in solution-processed deposited chloride–iodide perovskite film. The superior uniformity of the vapor-coated perovskite film results in a substantially improved PCE of 15.4%. In another work, Liu et al. [93] also found a smooth surface, good surface coverage, and better crystalline size uniformity with vapor process deposition.

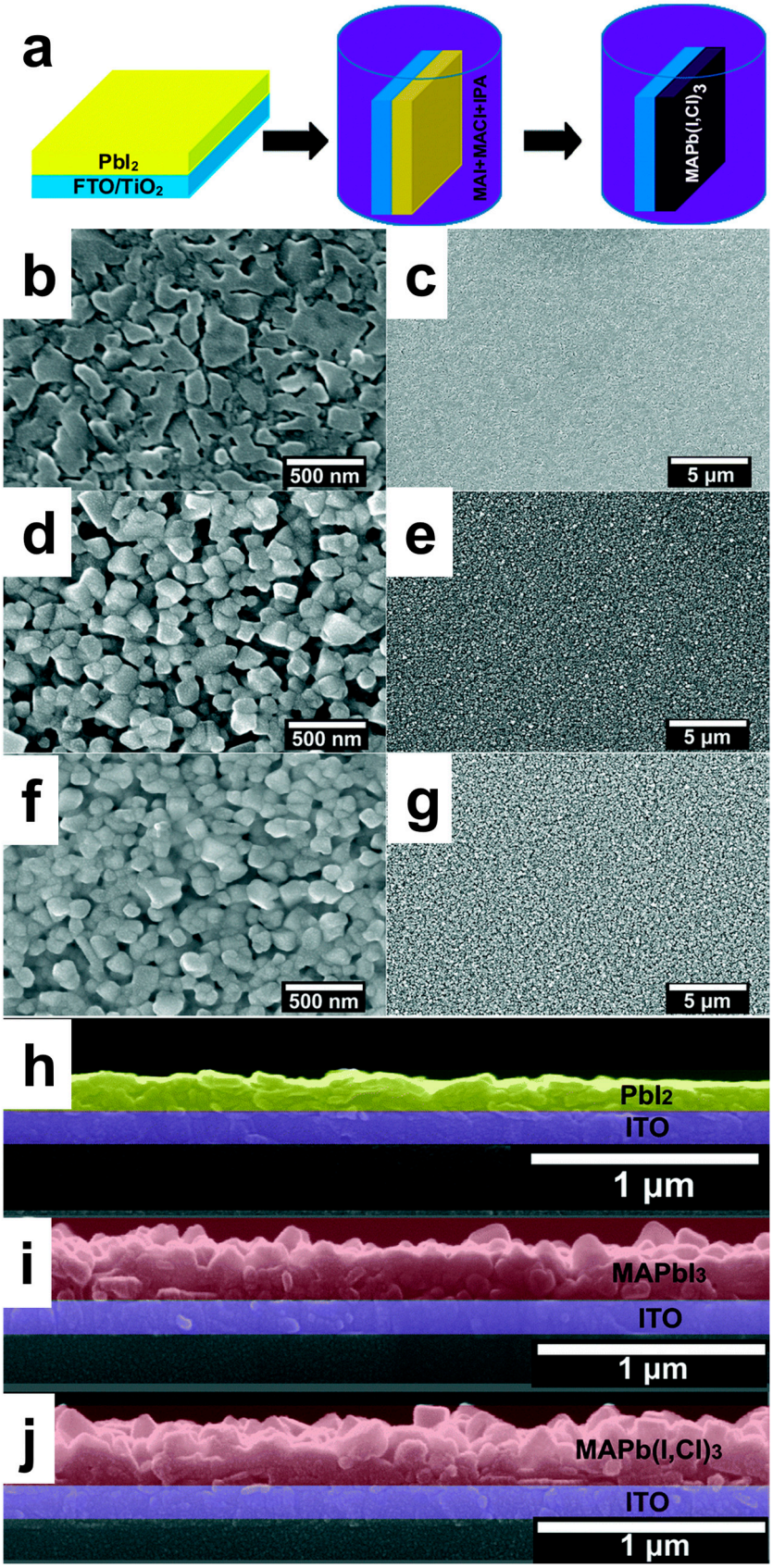

Figure 5. (**a**) Schematic diagram of the dip-coating process. Scanning electron microscopy images of PbI_2 (**b**,**c**,**h**), $MAPbI_3$ (**d**,**e**,**i**), and $MAPbI_{3-x}Cl_x$ (**f**,**g**,**j**) films. From [21].

However, a significantly long fabrication time due to limited reaction interfaces is a significant problem in vapor-phase deposition. It is also hard to control the evaporation rates of the multiple sources of perovskite precursors. This is why excessive consumption of the more volatile MAI is possible.

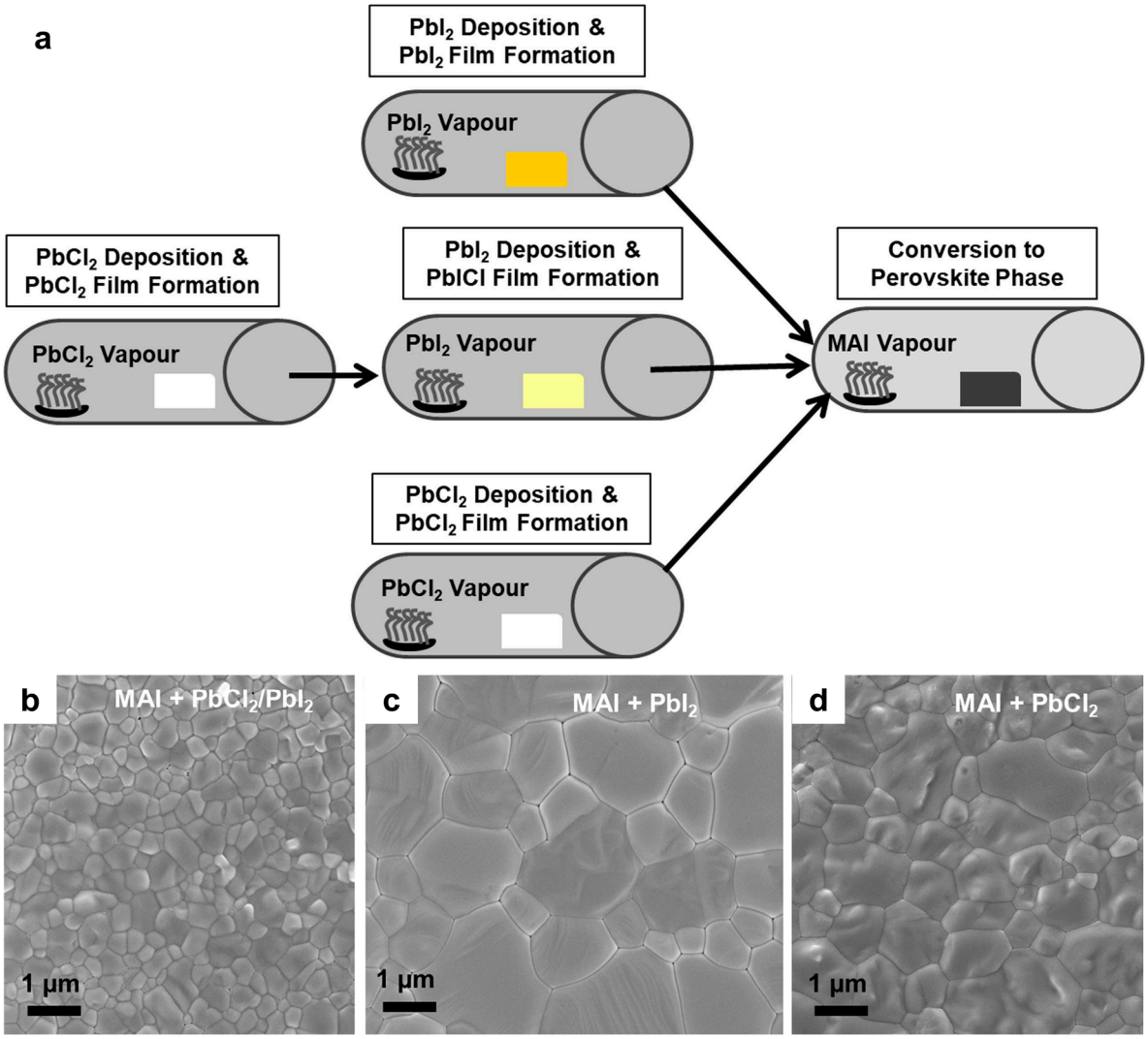

Figure 6. (**a**) Schematic representation of the chloride–iodide perovskite film deposition process with two-step and three-step vapor-phase deposition. Scanning electron microscopy images of chloride–iodide perovskite films from (**b**) three-step method, (**c**) two-step method, (**d**) two-step method [58].

3.4.3. Solution and Evaporation Process Deposition

Both the solution process and vapor-phase deposition have advantages and disadvantages. Some researchers used both approaches to incorporate Cl into I-perovskite films. $PbCl_2$ and PbI_2 have a solubility issue with dimethylformamide, so if the recipe has $PbCl_2$ or PbI_2, it is deposited with the vapor process. For example, Chen et al. [25] deposited $PbCl_2$ with thermal evaporation and dip-coated the film into the $MAPbI_3$ solution, which manifested a PCE of 15.12%. The final chloride–iodide film was obtained with the sequential repetition of this cycle (one cycle consists of vapor deposition and dip coating). In another work by Luo et al. [27], the MAI:MACl precursor was deposited through the vapor-phase deposition method on the spin-coated PbI_2 film. The PSC showed 1152 h of stability in ambient conditions without encapsulation. Jang et al. [55] fabricated a chloride–iodide perovskite film by the single-source vapor-phase deposition of $MAPbCl_3$ film and

a repeated spin coating of the MAI solution. This process helps to control the Cl/I ratio more precisely via subsequent anion exchange. The repetitive MAI treatment gradually fills the interstitial voids in the film. The average grain size was found to be up to 1.2 μm. The atomic Cl content in the film can also be controlled with the number of MAI treatments. Here, a maximum PCE of 19.1% was achieved.

In summary, solution deposition should be performed as the first step, with vapor deposition as the second step. The solution deposition step necessitates post-annealing treatment. This is why $PbCl_2$ or PbI_2 film should be deposited with the solution deposition step and as the first step. MACl or MAI should be deposited with the vapor deposition process as the second step because, in the second step, the chloride–iodide perovskite film is formed, and vapor process deposition does not necessitate any post-annealing treatment. Therefore, there is no probability of MACl escaping from the film.

3.5. Annealing Process Engineering

After solution process deposition, thermal annealing is usually necessary to fully convert the precursor film into perovskite. Thermal annealing helps to remove residual solvents and enhances crystallization and grain growth. The crystal structure, grain size, and film uniformity are optimized during heat treatment. Different morphologies can also be obtained, depending on the conditions employed during the thermal annealing process (duration, temperature, ambient atmosphere, etc.) [68].

The annealing process has a very crucial role in chloride–iodide perovskite formation. For example, Grätzel et al. [94] suggested that the Cl-doped state would not exist at too high an annealing temperature because the Cl^--ion-containing phase would melt at 103 °C. On the other hand, Dualeh et al. [95] found that a minimum temperature of 80 °C is required to ensure solvent vaporization and the perovskite material's crystallization. They also observed that increasing the annealing temperature to too high leads to the additional formation of PbI_2, which is detrimental to photovoltaic performance, as PbI_2 is insulating [96]. At lower annealing temperatures, the conversion to perovskite dominates following the reaction.

$$MAI + PbCl_2 \rightarrow MAPbI_{3-x}Cl_x + MACl \quad (19)$$

At higher annealing temperatures, there is the additional formation of PbI_2, as described as follows:

$$MAI + PbCl_2 \rightarrow MAPbI_{3-x}Cl_x + MAI + MACl + PbI_2 \quad (20)$$

If the $MAPbCl_3$ phase persists, Cl could leave the film as MACl during thermal annealing. $MAPbCl_3$ possesses lower formation energy and a lower boiling point than $MAPbI_{3-x}Cl_x$. It decomposes into $PbCl_2$ and MACl through annealing. MACl is more volatile than MAI. The escape of Cl results in undesirable vacancies and pinholes. From the above equations, residual MAI is found, which ultimately forms $MAPbI_3$. However, a small amount of extra $PbCl_2$ could facilitate the removal of excess MAI, even at low annealing temperatures [97]. In that case, a longer annealing time will be needed to properly form chloride–iodide perovskite. For example, Liu et al. [35] found that an excess Cl concentration in the precursor solution needs a longer annealing time. Ralaiarisoa et al. [98] witnessed that the domains containing the Cl-rich phase dominated in the early stage of annealing of the perovskite film. Only after sufficiently long annealing could one single perovskite phase with a homogeneous composition of Cl and I be found. The diffusion of Cl in the perovskite layer accompanies this composition evolution. Figure 7a shows a simple schematic representation of a cross-sectional image from time-of-flight secondary ion mass spectrometry. Here, in Figure 7a, it is illustrated that at the beginning of the annealing time, there are two different regions, namely, I-rich (region A) and Cl-rich (region B) regions. After a sufficient annealing time, completely homogeneous perovskite is formed

(see Figure 7b). The authors found an aggregation of Cl between the active and charge transport layers after full annealing, as shown in Figure 7b.

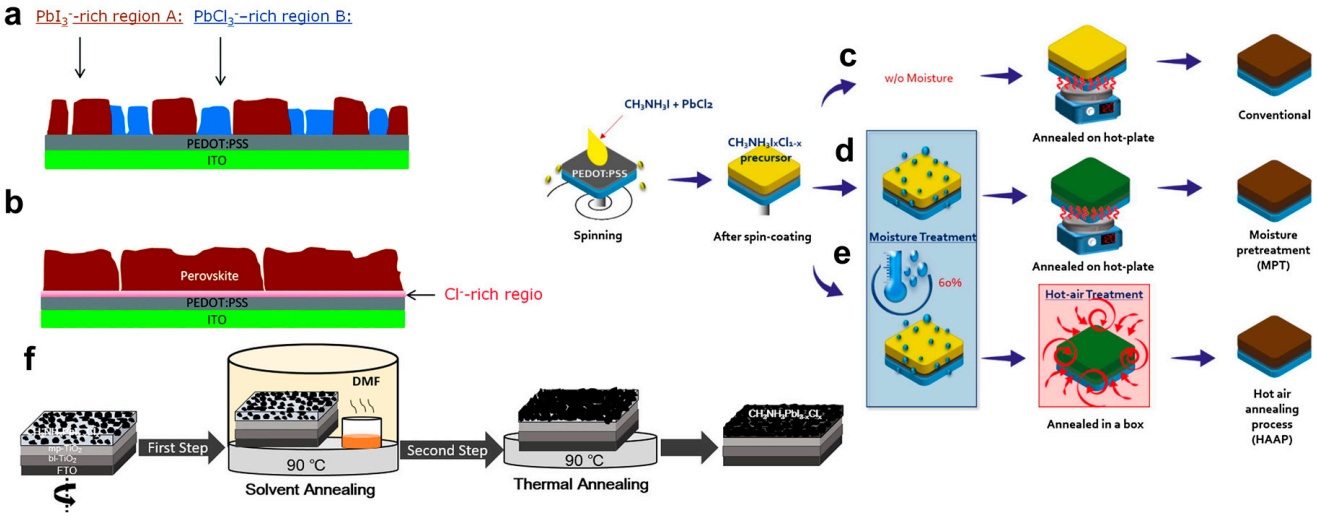

Figure 7. (**a**) Schematic cross-section of the lateral phase separation: region A corresponds to $MAPbI_3$, and region B corresponds to $MAPbCl_3$. (**b**) Homogeneous composition of chloride–iodide perovskite and Cl-rich region at perovskite interface and PEDOT:PSS [98]. (**c**) Conventional annealing process that does not involve moisture treatment. (**d**) Annealing process with moisture pretreatment. (**e**) Hot-air annealing process with moisture pretreatment [48]. (**f**) Schematic of the solvent-assisted annealing process of chloride–iodide perovskite film [28].

Therefore, it is a significant challenge to incorporate Cl into iodide perovskite. To deal with this issue, researchers tried a moisture-assisted annealing process. For example, Liu et al. [48] obtained a 15.55% PCE from chloride–iodide PSCs by employing moisture pretreatment before annealing and annealing in hot air. The entire fabrication process is illustrated in Figure 7c–e. The PCE increased from 9.05 to 11.87% when the moisture pretreatment process was used and from 9.05 to 15.55% when both moisture pretreatment and annealing in hot air were used. They explained the reasons behind the improved PCE with several chemical reactions, as follows:

$$MAI + PbCl_2 \rightarrow MAPbI_3 + MACl \quad (21)$$

$$MAI \rightarrow MA^+ + HI \quad (22)$$

$$MACl \rightarrow MA^+ + HCl \quad (23)$$

Since MACl is thermally unstable, it readily decomposes and is sublimated from the perovskite film, resulting in the final film not containing any Cl after the thermal annealing process. As MAI is hygroscopic, the solid MAI becomes a liquid when the perovskite precursor absorbs moisture during heat pretreatment. Consequently, this process decreases the MAI available to react with $PbCl_2$ during film formation. This incident results in some amount of Cl remaining in the final film. In addition, the generated MAI and hydroiodic acid serve as additives in the precursor film and enhance the crystallinity of the film. Finally, the remaining Cl can be incorporated into $MAPbI_3$.

There is also a relationship between moisture treatment and the annealing time. Cronin et al. [99] reported that humidity and the annealing time are closely interrelated for chloride–iodide perovskite film preparation. Both are vital factors that affect the performance of devices. A trade-off between humidity and the annealing time is required for optimal conditions. They proposed the following mechanism for perovskite formation:

$$MACl + PbCl_2 \rightarrow MAPbI_3 + MACl \quad (24)$$

Because MAI is hygroscopic, moisture exposure speeds up the conversion of the perovskite compound from the precursor and leads to faster grain growth [100,101]. Again, too much humidity can cause the degradation of $MAPbI_3$ as follows:

$$MAPbI_3 \rightarrow PbI_2 + MAI + HI \quad (25)$$

Too much humidity creates MAI and creates voids. Additionally, a long annealing time under high humidity increases the number of shunt paths in the film. They proposed a plot that enables the identification of the trade-off. The plot shows the response surface generated from the average efficiency of the cells. There are two input variables: annealing time and humidity.

Moreover, annealing the film in a solvent-induced environment helps Cl incorporation. Liu et al. [28] obtained chloride–iodide film with a grain size of up to 1.1 μm with a solvent-induced annealing process. The film was made from MAI, PbI_2, and $PbCl_2$, with a 4:1:1 molar ratio, and annealed in a dimethylformamide environment. The whole process is shown in Figure 7f. Here, a Cl-containing intermediate phase is formed, and MACl is released. The release of gaseous MACl assists in the crystallization and recrystallization of perovskite. During the annealing process in dimethylformamide, the chemical kinetics that takes place is suggested to occur in three steps.

Step 1:

$$MAI/MAPbI_3 + PbI_2 \quad (26)$$

Step 2:

$$MAI/MAPbI_{3-x}Cl_x + PbCl_2 + MACl + MAI \quad (27)$$

Step 3:

$$MAPbI_3 + PbCl_2 + MAI_2/MAPbI_{3-x}Cl_x + MACl + MAI \quad (28)$$

The intermediate phase delays the formation time of chloride–iodide perovskite. The delay is beneficial for the perovskite crystallization process [102]. This process promotes the migration and interdiffusion of precursor ions and molecules. This process is effective for Cl incorporation [103].

3.6. Device Structure Engineering

There are significant effects on the photovoltaic performance of chloride–iodide PSCs depending on whether they are porous (meso or nano) or planar alongside a regular (n-i-p) or inverted (p-i-n) structure [104]. In most high-efficiency devices, chloride–iodide PSCs have mesoporous structures. The mesoporous design facilitates the infiltration of perovskite. This is why thicker and more uniform perovskite films can be deposited on a porous (meso or nano) scaffold [68]. The mesoporous structure can selectively extract electrons from perovskite, further improving the photovoltaic performance. On the other hand, the planar structure has a comparatively simplified device structure but lower efficiency than the mesoporous structure [105]. The planar heterojunction is a more technologically viable architecture with large-scale manufacturability [68].

Docampo et al. [106] found a higher PCE from inverted porous PSCs than regular planar PSCs made with chloride–iodide perovskite films. In the mesoporous structure, the perovskite and charge transport layers are in close contact due to distributed heterojunctions, which allow efficient charge transfer over a short distance. On the other hand, in a planar structure with bulk heterojunctions, the photoexcited charges must travel through the whole film thickness to be collected by the electrodes. Therefore, the photoexcited charge recombination probability is much higher in the planar heterostructure. Again, the perovskite film thickness is crucial in optimizing planar heterojunction PSCs. A very thin film does not absorb sufficient sunlight. There is a substantial chance that the charge transport layers will not collect the photogenerated charge in a very thick film. In this case, there is a possibility that the electron–hole diffusion length will be shorter than the film thickness. Fortunately, the electron–hole diffusion length is greater than 1 μm in chloride–iodide perovskite. In contrast, iodide perovskite has a diffusion length of about 100 nm, mainly due to a much longer recombination lifetime [12].

In addition, X-ray photoelectron and ultraviolet photoelectron spectroscopy analyses of chloride–iodide perovskite films prove them to be n-type semiconductors [16]. This finding indicates high electron conductivity, which could lead to leakage current. Kelvin probe force microscopy measurement reveals that the Fermi level is closer to the center of the bandgap of chloride–iodide perovskite [21]. Therefore, there should not be a significant difference in PCE in chloride–iodide PSCs, whether in a regular or inverted structure.

4. Optimal Concentrations of Chlorine and Iodine

In this section, we will discuss the optimal concentrations of chlorine and iodine for improved efficiency and stability in chloride–iodide perovskite. The discussion is based on the data in Table 1.

4.1. Efficiency

Operational efficiency is a PSC's most crucial performance parameter, just like in other solar cells. There are two possible types of precursor combinations for preparing chloride–iodide perovskite: MAI/$PbCl_2$ or MACl/PbI_2. As $PbCl_2$ is less soluble than PbI_2, the MACl/PbI_2 combination is preferred. However, the PCE value is higher in MAI/$PbCl_2$ than in the MACl/PbI_2 combination, and MAI/PbCl2 is popular. Usually, the MAI/$PbCl_2$ combination with excess MAI (3 times the amount of $PbCl_2$, where the Cl concentration is 40%) is used. From Table 1, it is also found that most of the works used 40% Cl. This combination does not stoichiometrically reproduce a chloride–iodide perovskite film. Apart from that, a few of the works report optimal efficiencies with a 33% Cl concentration (MACl:PbI_2 = 1:1) and a 67% Cl concentration (MAI:$PbCl_2$ = 1:1). There are a couple of works reporting optimal efficiencies with a 25% Cl concentration with a molar ratio of MAI:PbI_2:$PbCl_2$ = 4:1:1. Again, this combination does not stoichiometrically reproduce a chloride–iodide perovskite film. Rao et al. [36] and Huang et al. [57] obtained an optimal PCE with a 10% Cl concentration (PbI_2:$PbCl_2$ = 9:1). Here, they varied the molar ratio of PbI_2:$PbCl_2$ from 1:9 to 9:1 with 1 molar MAI. Similarly, Mu et al. [33] obtained the highest PCE with a 7% Cl concentration. In Table 1, some cells for Cl concentration values are empty; these indicate that combined methods such as spin-coating–dip-coating, vapor-coating–dip-coating, etc., were used. This is why it is not easy to directly quantify the Cl concentration. Additionally, some authors added extra $PbCl_2$. Pham et al. [52] added 2.5% $PbCl_2$, which means 5% external Cl^- ions were used to obtain their optimal PCE. In a similar way, Cao et al. [53] added 5% $PbCl_2$ (10% Cl^- ions) to obtain the optimal PCE. Note that even for the same Cl concentration, the PCE values show anomalies, according to Table 1. There is no linear relationship between PCE and the Cl concentration, as most of the works improved their device performance in various ways, such as interface engineering and electron–hole transport layer engineering. They just followed their desired Cl concentration from the previous literature. In Table 1, we see that the best photovoltaic parameters of chloride–iodide PSCs are as follows: J_{sc} is 25.86 (mA/cm^2) [57], V_{oc} is 1.17 V [62], FF is

82.78 [54], and PCE is 21.23% [62]. It is noteworthy that the highest theoretical Shockley–Queisser-limit [107] performance parameters for the chloride–iodide PSCs are as follows: J_{sc} is 27.20 (mA/cm^2), V_{oc} is 1.28 V, FF is 90.2, and PCE is 31.4% [108]. Therefore, there are still many areas where it could be possible to improve the performance parameters.

4.2. Stability

There is a concern about whether PSCs will be stable for the decades expected for commercialization [109–111]. Without improving the stability, it will not be possible to transfer them from the laboratory to the industry, even if they possess lucrative efficiencies. Their long-term stability has become the most crucial question. Their stability is still an unresolved challenge for their outdoor applications [112,113]. Undesirably, perovskites possess an intrinsically unstable nature [114]. Specifically, they have the propensity to be sensitive to certain ambient outdoor conditions [115–117]. Their stability degrades upon severe environmental conditions, e.g., humidity, heat, and light [118–120]. These conditions seem to be the bottleneck that hinders their further commercialization [119]. To achieve a highly stable device, the degradation mechanism of perovskite materials should be investigated [121,122]. In addition, they need to pass accelerated aging tests under different stressful conditions if we want to commercialize them. Widespread accelerated aging tests include light soaking at temperatures from 60 °C to 85 °C with 85% relative humidity for at least 1000 h [123]. While reasonable efficiency has been demonstrated, as is found in Table 1, the stability issue of chloride–iodide PSCs is almost wholly ignored. This is why finding the relation between stability and the Cl concentration is difficult. However, Naoki et al. [124] developed a model of the degradation mechanism of chloride–iodide perovskite solar cells. At the same time, they explored the effect of adding a small amount of extra PbI_2/$PbCl_2$ on the stability of chloride–iodide perovskite solar cells. They used three different types of samples with a common molar ratio of MAI:$PbCl_2$ (3:1) for their experiment. The first one had an extra 10% PbI_2, which is denoted as (+PbI_2), the second one had an extra 10% PbI_2 + 5% $PbCl_2$, which is denoted as (+PbI_2 +$PbCl_2$), and the third one had an extra 10% PbI_2 with a higher concentration, which is denoted as (+PbI_2 (HC)). A schematic depicting the carrier transport and decomposition mechanisms for chloride–iodide perovskite crystals is illustrated in Figure 8. The grain size of the ((+PbI_2 (HC)) sample is larger than that of the (+PbI_2) sample, whereas the grains are in the most compact form in the (+PbI_2 +$PbCl_2$) sample. When all the samples are exposed to ambient air, MA^+ and HI desorb from the surface of the perovskite layer, and the perovskite crystals decompose into PbI_2 crystals at the interface of perovskite/spiro-OMeTAD. There is also the possibility of $PbCl_2$ formation, although the Cl concentration is much lower than the I concentration. It is important to add that PbI_2 and $PbCl_2$ are a little bit insulating in nature. The PbI_2 crystals that are formed on the perovskite surface work as nuclei, and this process is harnessed by the addition of extra PbI_2. This phenomenon reduces the decomposition of the perovskite crystals at the perovskite surface, enhances the smoothness of the perovskite/spiro-OMeTAD interface, and increases the distribution density of perovskite grains. From the stability test, it was found that the extra-Cl-containing one was the most stable, which suggests that Cl doping effectively stabilizes the PSC.

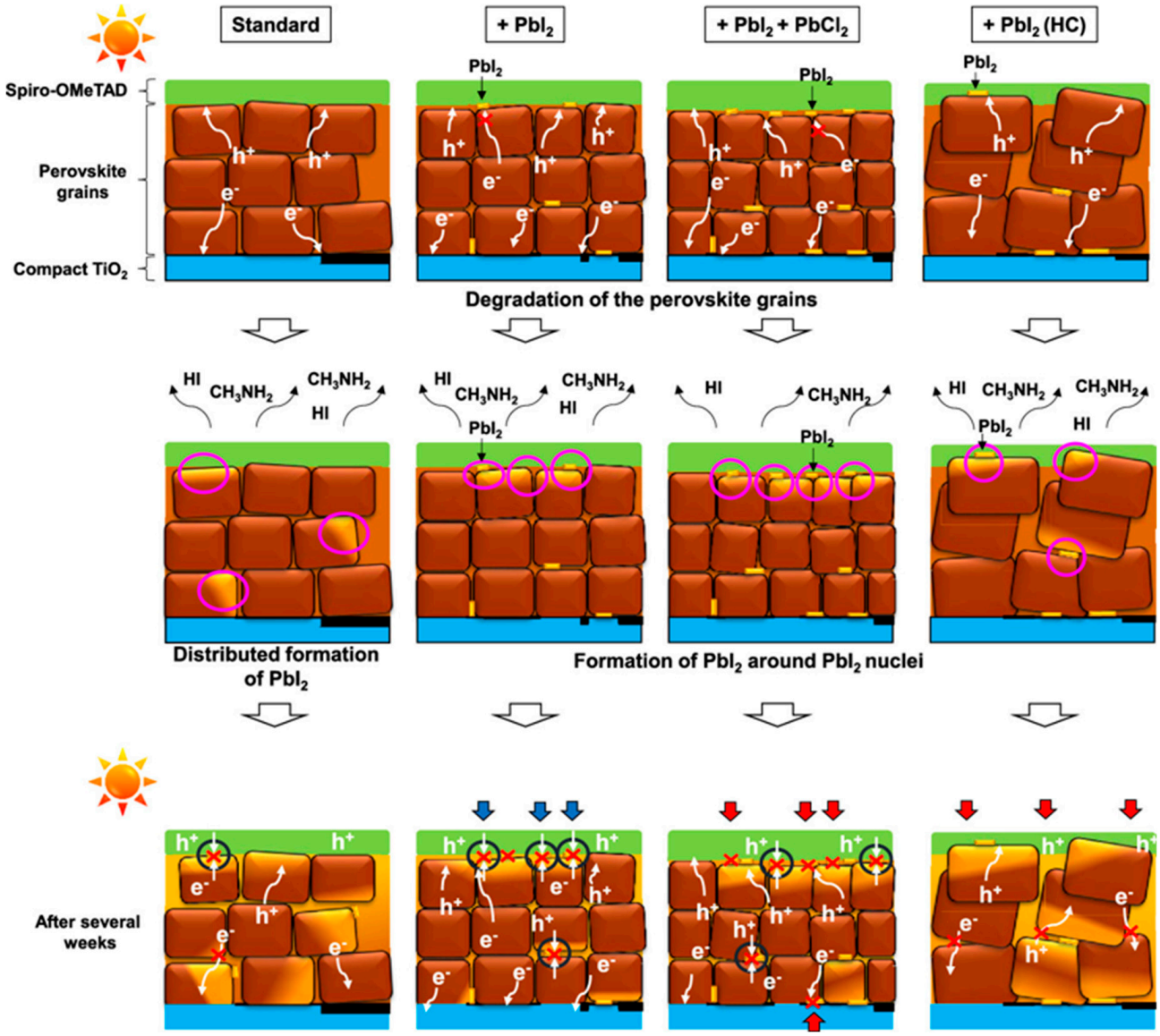

Figure 8. Schematic representation of decomposition and carrier transport mechanism of chloride–iodide PSCs [124].

5. Challenges of Chloride–Iodide PSCs

Here, we discuss different issues that can affect the efficiency and stability of chloride–iodide PSCs and Cl's role in mitigating them. The significant challenges of chloride–iodide perovskite can be divided into two groups: intrinsic factors, such as phase segregation, radius mismatch, Cl sublimation, etc., and extrinsic factors, such as moisture, heat, light, etc.

5.1. Chlorine and Iodine Phase Segregation

Phase segregation is a common phenomenon in mixed-halide perovskites and is severe in chloride–iodide perovskites. Obtaining a continuous, properly distributed chloride–iodide solid-phase film is a big challenge for chloride–iodide PSCs. Excessive co-existing wide-bandgap $MAPbCl_3$ will generate fewer photogenerated electron–hole pairs, inhibit electron transfer, and deteriorate the photovoltaic performance [72]. Phase segregation in chloride–iodide perovskite can occur at two different times. One is during the film's growth, and another one is during the film's annealing.

The materials are usually self-assembling during film growth, and the constituent components explore diverse possible configurations during the assembly process. They choose the weakest bonding interactions to find the most energetically favorable one. As a result, heterogeneous nucleation sites can occur instead of homogeneous nucleation. For example, Tidhar et al. [65] found that $PbCl_2$ in the perovskite precursor solution has a remarkable effect on perovskite synthesis. During the fabrication process, $PbCl_2$ forms nanocrystals. These nanocrystals act as heterogeneous nucleation sites at the time of the formation of perovskite crystals in the solution. Thus, if the system has both PbI_2 and $PbCl_2$, there is a possibility of the formation of two different phase domains, such as $MAPbI_3$ and $MAPbCl_3$.

The phase segregation process continues even after film growth during annealing. Williams et al. [75] found discrete nucleation immediately upon deposition and the initial annealing of the chloride–iodide perovskite film. They observed discrete $PbCl_2$ nucleation directly after deposition, as shown in Figure 9a. They identified a Cl-rich region near the substrate during annealing, depicted in Figure 9b. After complete annealing, they also observed segregated Cl and I phases (see Figure 9c). Qiao et al. [69] reported that the chloride–iodide perovskite single crystal is metastable and decomposes over time into $MAPbI_3$ and $MAPbCl_3$ phases based on time-dependent X-ray diffraction and nuclear magnetic resonance. Mamun et al. [44] took the photoluminescence spectrum of a chloride–iodide perovskite film and found it to be asymmetric in shape. The photoluminescence spectrum was deconvoluted using a bi-Gaussian function, representing the presence of segregated phases ($MAPbI_3$ and $MAPbCl_3$). They also performed photoluminescence mapping and observed that the segregated phase mainly comes from the grain boundaries.

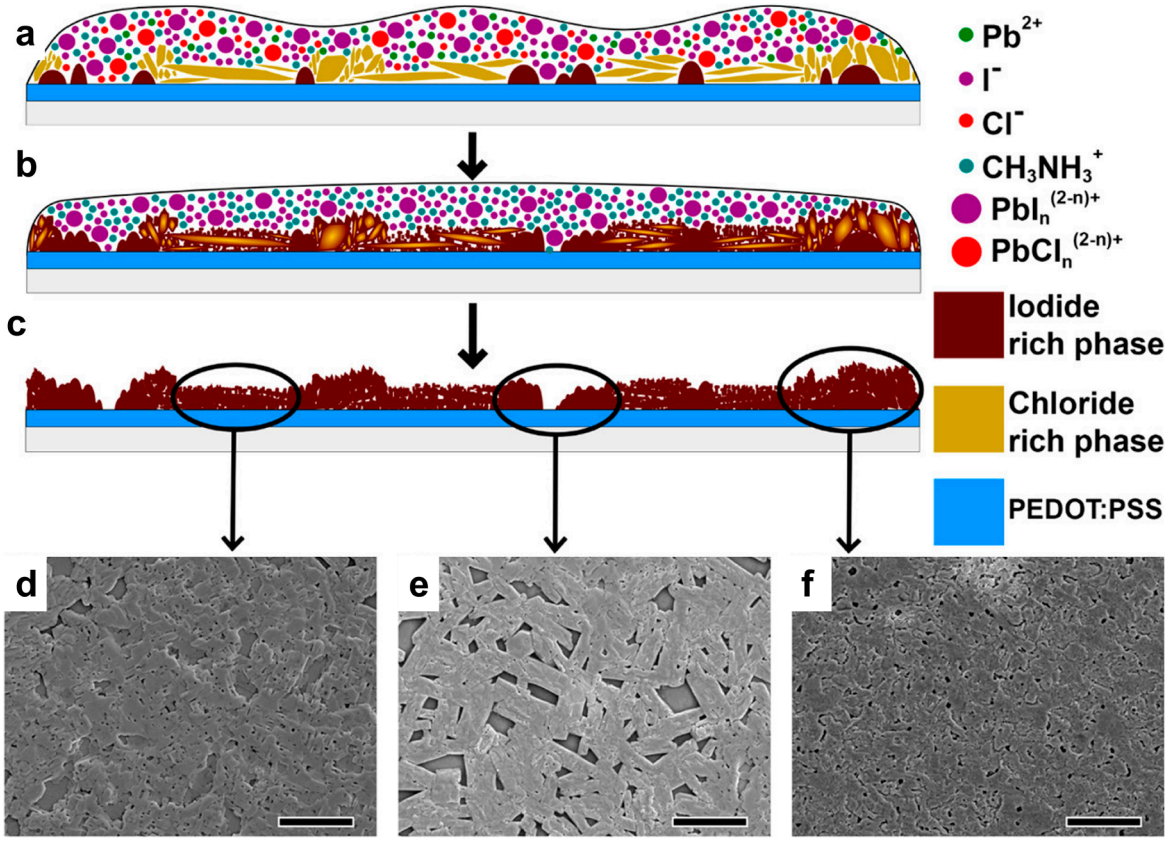

Figure 9. Schematic representation of chloride–iodide perovskite film: (**a**) nucleation during deposition, (**b**) phase evolution, and (**c**) growth during annealing. (**d**–**f**) Scanning electron microscopy images that are representative of the three major morphological constituents (scale bars are 2 μm) [75].

$MAPbI_3$ and $MAPbCl_3$ correspond to two crystalline phases at room temperature: tetragonal and cubic. Two different crystalline phases and local oriental heterogeneity due to phase segregation might cause local residual stress and strain. Generally, the stress and strain concentrate at the grain boundaries. The presence of local stress and strain facilitates the formation of vacancies. These vacancies might initially create shallow defects, turn into deep traps via charge transfer with oxygen or water molecules, and accelerate perovskite degradation in ambient conditions [125]. Therefore, the generation of Cl vacancies might be further fueled. The typical route for trap passivation is based on Lewis acid–base chemistry approaches due to the ionic nature of perovskites. The Lewis acid–base adduct approach is helpful for defect passivation [126]. A Lewis acid capable of accepting a pair of nonbonding electrons can passivate electron-rich defects. In that case, extra Cl^- ions can be added to the perovskite precursor solution [127]. Saidaminov et al. found that a small amount of Cl substitution could reduce the lattice strain of $FAPbI_3$ and suppress defect formation [125].

5.2. Chlorine and Iodine Radius Mismatch

It is well known that there is a radius difference between chlorine and iodine. Iodine is bigger than chlorine. It is believed that small-size Cl's incorporation to replace larger-size I makes the unit structure more compact. This should reduce I^- ion migration. At the same time, due to the size mismatch, it is challenging to incorporate Cl^- ions and reduce Cl^- ion migration. Ion migration is one of the most thought-provoking and mysterious phenomena in perovskite devices and leads to poor stability. This intrinsic phenomenon in perovskite materials occurs owing to their ionic conducting nature. One of the primary routes of ion migration in perovskite is the availability of vacancies (Schottky, Frankel, etc.) in the crystal [128,129]. For example, I^- ions might easily migrate through the polycrystalline perovskite grains and even out the perovskite layer through interference with the metal electrode [130]. Huang et al. [131] employed photothermal-induced resonance microscopy to map the distribution of ions in a perovskite film. The measurements demonstrate the movement of the MA^+ cation under an external electric field. In another work, Huang et al. [132] measured energy-dispersive X-ray spectroscopy under an external electric field on a perovskite film. The above discussion indicates the easy movement of I^- ions in perovskite films. It is believed that the mobile I^- ions will not return to their original positions in the lattice. Compared to the original perovskite structure, the redistributed one should have more residual stress and strain within the lattice and thus results in poorer stability. The iodide ion has the lowest defect activation energy of 0.58 eV, indicating that the vacancy-mediated diffusion of the I^- ion is most favorable. At the same time, the activation energy of the MA^+ cation is found to be higher, and the value is 0.84 eV. The activation energy of the Pb^{2+} ion is as high as 2.31 eV, indicating that the Pb sublattice is immobile, which should not be connected to ion migration [133,134].

Additionally, a strange I-V hysteresis phenomenon is observed for PSCs. The variations in the I-V characteristics depend on the direction and voltage sweep rate [135]. The origin of hysteresis is still an open debate, although I^- ion migration is considered one of the main culprits. I^- ion migration results in charge traps and an imbalance in the number of electrons and holes, which might produce ferroelectricity. Figure 10 shows various origins of hysteresis that occur in PSCs. Hysteresis raises a significant concern, as it undermines the accuracy of the measured efficiencies of these devices. Hysteresis is also considered a hindrance to stable PSCs since it strongly affects the reliability of the device's photovoltaic performance under practical conditions [136].

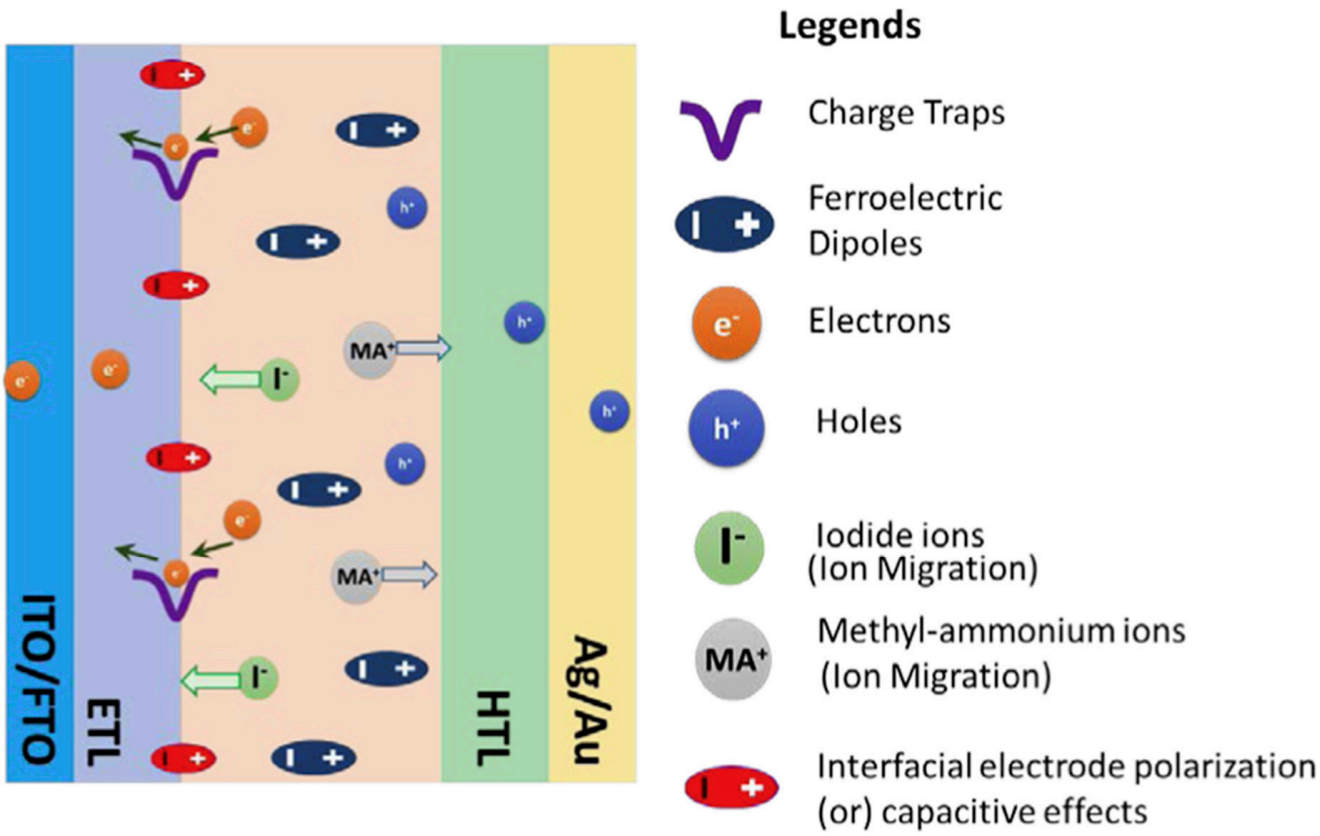

Figure 10. Schematic diagram of the various possible origins of hysteresis in PSCs [137].

Under light illumination, a perovskite film absorbs photons and generates electron and hole charge carriers. The photogenerated electron and hole are selectively separated and collected by the cathode and anode, respectively. An ohmic contact between the semiconductor and metal electrode is preferred to obtain efficient charge carrier collection to reduce the interfacial energy barriers for charge transfer at the contact. Therefore, p-i-n-structured PSCs commonly employ a metal electrode with a low work function, such as Al and Ag, while a metal electrode with a high work function, such as Au, is preferred for n-i-p-structured PSCs [138]. There is a possibility of the diffusion of I^- ions or metal particles into the perovskite layer and their reaction. For example, Ag and Al might react with I in perovskite and form AgI [139] and AlI_3 [140], respectively. These phenomena strongly affect the long-term device stability of PSCs.

Therefore, the primary strategy to mitigate the detrimental effect of mobile ions is enhancing the chemical bonding among perovskite elements [140]. Table 1 shows that in most of the chloride–iodide PSCs, small hysteresis is observed. Saidaminov et al. [125] suggested that incorporating Cl suppresses the density of vacancy defects by lattice strain relaxation. Strain originated from the size mismatch between MA^+ or FA^+ and the lead halide cage. Strains result in cage distortions, tilting PbI_6 or $PbCl_6$ octahedra, and the formation of halide vacancies. The lattice strain can be reduced by incorporating small ions such as Cl. Hence, Cl addition can effectively mitigate the appearance of vacancy defects in chloride–iodide perovskites. Their PSC (unencapsulated) exhibits a slow PCE degradation rate (loses 0.25% per min) under one sun illumination with a relative humidity of about 50%. In comparison, Cl-free PSC fails at 1.5% PCE per min, meaning faster degradation.

Cl incorporation into I-perovskite results in a more compact, strain- and stress-free crystal structure. The Pb-Cl bond is stronger than the Pb-I bond [141]. As a result, there is a lower concentration of iodide ions to react with the metal contact.

5.3. Chlorine Sublimation during Annealing

The literature survey found that the most popular recipe for chloride–iodide perovskite is a 3:1 molar ratio of MAI:$PbCl_2$. As about a three-fold higher quantity is used, there is a possibility that extra MAI remains. The remaining MAI can be transformed into $MAPbCl_3$. The boiling temperature and formation energy of $MAPbCl_3$ is lower than the average annealing temperature of perovskite. As a result, $MAPbCl_3$ decomposes into MACl. MACl is too volatile. This is why, during annealing, MACl escapes from the film. This phenomenon results in Cl vacancies, which are detrimental to PCE. A detailed discussion on this topic is presented in Section 3.5.

5.4. Moisture Effect

Moisture or humidity (H_2O) in ambient air affects the chemical stability of PSCs. Nearly all research groups perform perovskite deposition in a dry atmosphere to avoid ambient exposure during device fabrication. Ensuring a dry atmosphere is not feasible or cost-effective for the large-scale production of PSCs.

The rapid degradation of chloride–iodide perovskite due to humidity can be observed from its color change from dark brown to yellow. Specifically, $MAPbI_3$ perovskite is prone to react with moisture in the surrounding atmosphere. Highly hygroscopic MAI cations suck up water from the environment. $MAPbI_3$ transforms into aqueous MAPbI, and there is also solid PbI_2 (PbI_2 is insulating in nature and hinders efficient charge transmission) remaining, which is shown as follows [142]:

$$MAPbI_3 + H_2O \rightarrow MAPbI + PbI_2 + H_2O \quad (29)$$

During this phenomenon, perovskite partially dissolves and forms hydroiodic acid. The following chemical reactions describe the degradation of aqueous MAPbI induced by moisture [143].

$$MAPbI \rightarrow MAI + HI \quad (30)$$

In the case of oxygen exposure, the above degradation speeds up as the bonding strength between the MA^+ cation and hydrogen is reduced [144]. In the presence of oxygen, hydroiodic acid transforms into iodine and water components as follows:

$$HI + O_2 \rightarrow I_2 + H_2O \quad (31)$$

In the presence of ultraviolet radiation, hydroiodic acid breaks down into hydrogen and iodine as follows:

$$HI \rightarrow H_2 + I_2 \quad (32)$$

The degradation process of $MAPbI_3$ with moisture follows several consecutive steps: surface passivation, free electron doping, interfacial hydration, and bulk hydration. $MAPbI_3$ contains uncoordinated bonds that serve as charge traps and exist on the surface and grain boundaries. When moisture comes into contact with the surface of $MAPbI_3$, the moisture can rapidly form hydrogen bonds with uncoordinated iodine atoms on the surface. As a result, a continuous network composed of water molecules that overlay the perovskite surface is formed. The water molecular network donates free electrons to the bulk perovskite as effective n-type doping. Gradually, moisture penetrates through the surface of the perovskite. Surprisingly, an intermediate low-dimensional hydrated perovskite layer protects the bulk perovskite from moisture during this process. This phenomenon may be why some devices fabricated in certain humid environments can enhance photovoltaic performance [143].

The partial substitution of Cl for I in $MAPbI_3$ helps the stability of the device in humidity [145,146]. Fabrication in humid ambient air or with a little water added to the perovskite precursor solution helps to grow quality chloride–iodide perovskite films. The boiling temperature of the water is lower than that of dimethylformamide. He et al. [49] found that water can resist the decomposition of the perovskite film and weaken iodide ion migration, enhancing the device's stability in the atmospheric environment. A PSC device with 1.5% water added maintained a PCE of 12.01%, higher than that (1.64%) of the reference device, after being stored in the air for 120 h. The PCE of a PSC with water added is 14.02%, higher than that (11.17%) of the reference device without water added. Figure 11a shows the operation process for preparing PSCs in ambient air with water added. Figure 11b shows the variation in key performance parameters of PSCs without and with 1.5% H_2O. Another alternative is adding a hydrophobic inorganic precursor such as CsCl as an additive [147–151]. The inorganic precursor will act as a water-repelling additive to promote moisture resistance and increase the hydrophobicity of the component [152].

5.5. Heat Effect

Besides moisture stability, thermal stability is another fundamental concern for PSC commercialization. There are two possible thermal effects on the stability of chloride–iodide PSCs: phase transition and chemical degradation.

In normal practical conditions, direct exposure to sunlight (e.g., 100 mW/cm^2 in full sun) increases the solar panel temperature. Heat accumulation can raise temperatures to as high as 85 °C because of continuous exposure to sunlight illumination. Thus, for PSCs working under sun illumination, the temperature of the solar cells is greater than the phase transition temperature for $MAPbI_3$ from the tetragonal to cubic phase [92]. When sunlight is absent, the solar panel temperature decreases toward the normal ambient phase transition temperature from the cubic to tetragonal phase. This cyclic phase transition affects the photovoltaic performance of solar cells. It is hoped that with the addition of a chloride base precursor to iodide perovskite, the phase transition process does not occur. This would ultimately enhance the stability of the solar cells.

Furthermore, perovskites decompose into their original precursor elemental components when heated [68]. Conings et al. [153] found that degradation occurs at 85 °C even in inert conditions. To better understand thermally induced degradation, they calculated the formation energy per unit cell in chloride–iodide perovskite. They found values of around 0.11–0.14 eV. The thermal energy (0.1 eV) estimated at 85 °C is close to this formation energy. Hence, the degradation of chloride–iodide perovskite at 85 °C is expected. However, Xu et al. [72] found that for Cl contents, about 10% could help to improve the thermal stability of chloride–iodide perovskite. Chae et al. [154] also observed that the chloride–iodide perovskite film was thermally stable up to 140 °C for a Cl concentration of less than 5%.

5.6. Light Effect

$MAPbI_3$ also shows chemical degradation when exposed to ultraviolet light. Photoinduced ion migration, halide segregation, and chemical degradation are expected consequences of prolonged light illumination on perovskites [155]. Light produces hydroiodide from $MAPbI_3$. The following chemical reaction happens on $MAPbI_3$ upon ultraviolet light exposure.

$$MAPbI_3 \leftrightarrow PbI_2 + MAI + HI \quad (33)$$

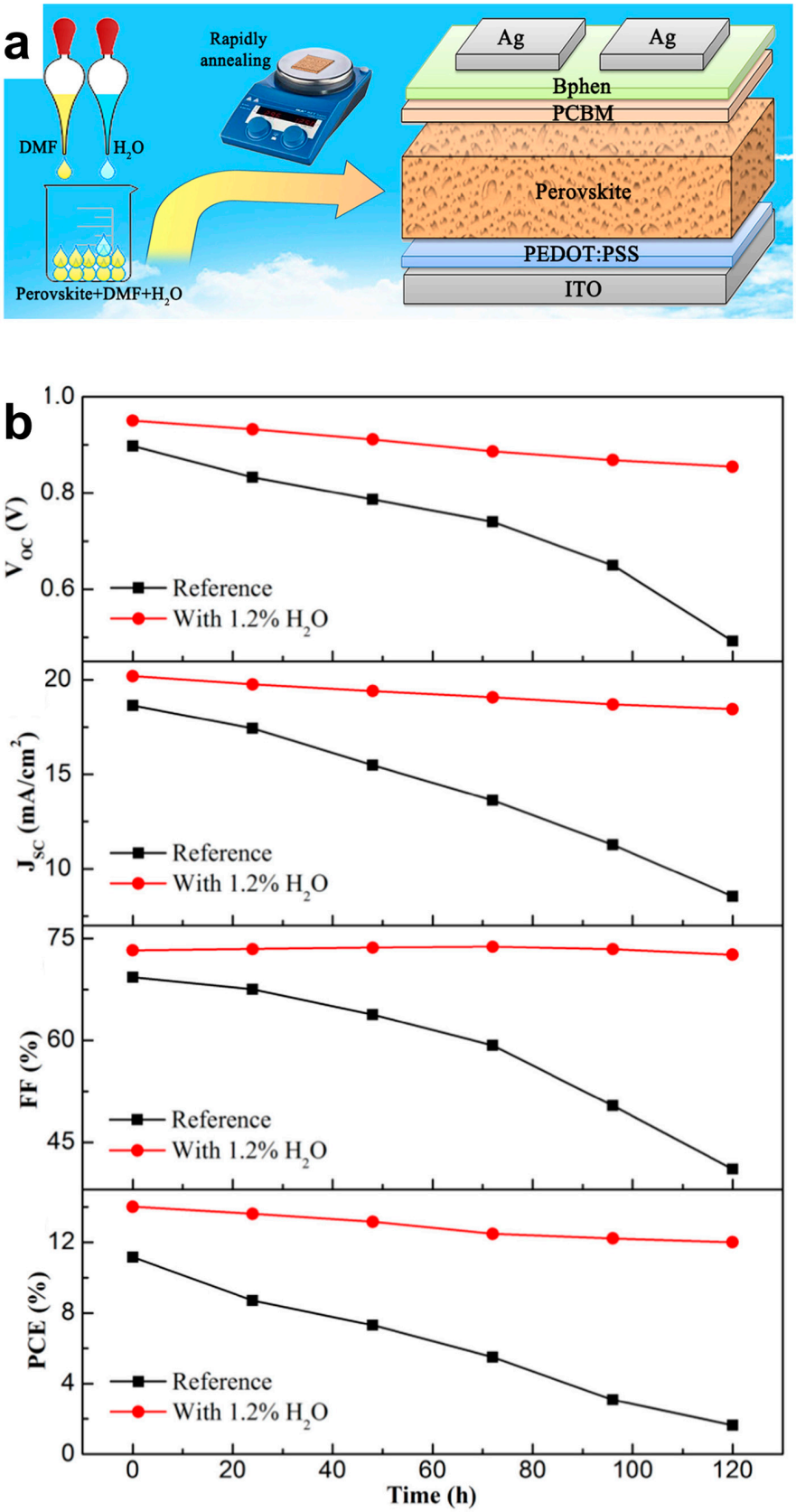

Figure 11. (**a**) The operation process chart of preparing PSCs with water added in ambient air. (**b**) The variation in key performance parameters without and with 1.5% H_2O [49].

In the presence of oxygen, iodine is generated from the remaining MAI, and the process can be described as follows:

$$MAI + O_2 \rightarrow MAI + H_2O + I_2 \quad (34)$$

The remaining MAI can also transform into iodine in the presence of carbon dioxide as follows:

$$MAI + CO_2 \rightarrow MAI + HCO_2 + I_2 \quad (35)$$

Recent work demonstrates that photoinduced chemical degradation is largely suppressed by directly alloying with 2 to 5% Cl into the lattice of FAC-based perovskite [156]. The resulting PSC maintains 96% of the initial PCE after 1000 h in a N_2 atmosphere.

6. Conclusions

In conclusion, Cl incorporation with I-based perovskites enhances efficiency and the device's stability. Usually, Cl preferentially aggregates near the interface of the perovskite and charge transport layers, which helps efficient interfacial charge extraction. The bonding strength of Pb-Cl is higher than that of Pb-I. Thus, Cl incorporation should produce a more compact crystalline structure. Cl improves crystallographic texture, crystalline orientation, and polycrystalline morphological aspects. Incorporating a small amount of Cl into I-perovskite could transform the crystal phase from tetragonal to a more stable cubic phase at room temperature. These optoelectrical and morphological improvements help to enhance the photovoltaic performance.

From the above review, it can be concluded that the probability of miscibility between Cl and I is too low because of phase segregation, a significant difference between their ionic radii, the sublimation of Cl during annealing, etc. Due to phase segregation, different chloride and iodide perovskite phase domains are created in the chloride–iodide film. Chloride perovskite has a cubic structure, and iodide perovskite has a tetragonal structure at room temperature. These different phase structures in the same film create local stress and strain in the film and cause instability. Due to the low miscibility of Cl with I, the chloride–iodide phase is either metastable or possesses higher formation energy. Again, Cl can escape from the film in the form of MACl, and the creation of Cl vacancies could also make the chloride–iodide perovskite unstable. As shown by the above review, different methods have been followed in various studies in the literature to discover how to incorporate chlorine into iodide perovskites and make them stable. We now discuss some possible strategies to solve this issue.

1. Different molar ratios of precursors, such as MAI, MACl, PbI_2, $PbCl_2$, etc., are usually used to fabricate chloride–iodide perovskites. Excess MA^+ ions produce unwanted MACl. MACl escapes from the film during annealing and creates Cl vacancies. In contrast, extra Cl contents result in a poorer PCE. It is found from Table 1 that a 5–10% Cl concentration is the optimal condition. However, in most of the literature, the Cl concentrations that are calculated for the precursor solution and measured in the film are not the same. Therefore, it is necessary to identify a more accurate molar ratio. Another way is to add 5–10% extra PbI_2 to the chloride–iodide perovskite precursor solution. By adding PbI_2, the recombination of electrons and holes should be reduced [157].
2. Different Cl-containing additives can be used, especially those with bigger cation sizes than MA^+ or FA^+ cations. These additives would introduce only Cl^- ions in the system. However, regarding the role of cations such as MA^+ and FA^+ in the additive, the cation needs to be large enough not to be incorporated into the lattice and thereby maintain the pristine perovskite bandgap. Additives such as ammonium chloride [158], poly ammonium chloride [159], etc., would be better candidates.

3. Takeo et al. [160] found the best PCE with the chloride–iodide-based PSC fabricated at 140 °C. This is because in a temperature range of 130–150 °C, even in ambient air conditions, the humidity effect should be reduced. At the same time, this temperature would provide sufficient diffusion and interaction between the reactants for perovskite formation. In the case of chloride–iodide perovskite, annealing leads to the sublimation of Cl in the form of MACl. Specifically, annealing at more than 100 °C could initiate Cl sublimation. At the same time, at least 80 °C is necessary for perovskite crystallization. Therefore, to overcome this problem, annealing in the presence of moisture or solvents such as dimethylformamide can be performed to help reduce Cl sublimation.
4. Dangling bonds on the perovskite film surface are responsible for the creation of surface states. These surface states work as trap states and increase nonradiative recombination. Thus, the V_{oc} voltage is reduced, as well as the PCE. Again, grain boundaries in the polycrystalline thin film work as a permeation route for oxygen and moisture. Thus, they severely impact the stability of PSCs. Therefore, it is clear that the surface is a critical point for efficiency and stability. To solve these issues, interface engineering is a good option. It is possible to passivate positively and negatively charged defects by utilizing the Lewis acids and bases. In this regard, various functional groups, especially ligands (bidentate anilinium [161], ethylenediamine [162], etc.) are very effective passivators. As the halogen site of perovskite works as a Lewis base, any ligands that have Lewis acids will interact with each other. The electronegativity of chlorine is higher than that of iodine. Thus, the chlorine content in perovskite would facilitate more efficient interaction with Lewis acids. Another bottleneck of PSCs is the unprotected vertical side of the perovskite thin film. Moisture and water can easily penetrate through this lateral side. Post-device ligand treatment could effectively reduce this problem and increase the stability of PSCs. In post-device ligand treatment, ligand vapors will induce chemical modification in the selected lateral regions of the perovskite layer. This prevents the diffusion of moisture and oxygen into the protected active perovskite region, thus enhancing the PSC stability. For example, diethylenetriamine molecules can interact with $MAPbI_3$ via the substitution of MA^+ [163]. We know that in chloride–iodide perovskite, excess MA^+ reacts with Cl^- and forms MACl as a byproduct, which is not desirable. Through post-device ligand treatment, diethylenetriamine molecules reduce the quantity of MA^+ and thus decrease the formation of MACl.
5. HTL materials are crucial for the stability of the PSC. To date, Spiro-MeOTAD, P3HT, and PEDOT:PSS are usually used as HTL materials and can be deposited through cheap solution process deposition. Spiro-MeOTAD and P3HT are costly materials, although Spiro-MeOTAD is the most used HTL material. LiTFSI salt doping in Spiro-MeOTAD is needed to increase p-type conductivity. LiTFSI is a hydrophilic salt and is considered the main reason for the moisture-induced degradation of Spiro-MeOTAD. Again, in the case of chloride–iodide perovskite, there is a possibility of the formation of LiCl, which is hygroscopic and could affect the stability of the PSC. On the other hand, PEDOT:PSS is a comparatively cheap material, although it needs high annealing temperatures to remove water content. Thus, an annealing-free dry deposition process of PEDOT:PSS would be a good option. Oxidative chemical vapor deposition is an alternative option to deposit conductive polymers in dry conditions [164]. In this powerful method, polymerization, doping, and thin-film formation are possible to perform simultaneously. The mild fabrication conditions permit the direct deposition of polymer conducting layers onto thermally sensitive substrates.

6. The biggest challenge for PSCs is to transfer them to the industry from the laboratory. To date, almost all efforts to improve their efficiency and stability have been on the laboratory scale and, of course, used cheap solution process methods. In laboratory-based small-size PSC fabrication with spin coating, researchers are struggling to make defectless interfacial contacts, as well as bulk films. Due to their small size, it is somewhat manageable to fabricate perovskite thin films with fewer defects, whereas, for large-size solution-based PSCs, slot-die coating is popular. For large-size solution-based PSC fabrication, controlling the defect density is very challenging. One possible way is to make thicker films, which will have a lower defect density. In this case, chloride–iodide perovskite offers an advantage for large-size commercial production. The carrier diffusion length is much longer for chloride–iodide perovskite compared to other types of perovskites. Again, another challenge is to control the surface roughness factor. A smoother surface has a lower roughness factor. For chloride–iodide perovskite preparation, there is a problem of the low solubility of PbI_2 and $PbCl_2$, even in DMF. In this case, two-step slot-die coating would be a possible solution. Chang et al. [165] prepared three types of solutions with PbI_2—with only DMF, with both DMF and DMSO, and with only DMSO—in a two-step fabrication process to fabricate $MAPbI_3$ films. They found a colloidal-like PbI_2 solution with only DMSO and a much smoother surface with a lower surface roughness factor. Therefore, one possible way to overcome the problem is to make a $PbCl_2$ colloidal solution in DMSO and deposit it on the MAI film in a two-step slot-die coating process.

Author Contributions: Conceptualization, A.U.; methodology, A.H.H.; validation, A.U.; formal analysis, A.H.H.; investigation, A.H.H.; resources, A.U.; data curation, A.H.H.; writing—original draft preparation, A.H.H.; writing—review and editing, A.H.H.; visualization, A.H.H.; supervision, A.U.; project administration, A.U. All authors have read and agreed to the published version of the manuscript.

Funding: This research received no external funding.

Data Availability Statement: Not applicable.

Conflicts of Interest: The authors declare no conflict of interest.

References

1. Elumalai, N.K.; Mahmud, M.A.; Wang, D.; Uddin, A. Perovskite Solar Cells: Progress and Advancements. *Energies* **2016**, *9*, 861. [CrossRef]
2. Zhu, X. The Perovskite Fever and Beyond. *Acc. Chem. Res.* **2016**, *49*, 355–356. [CrossRef] [PubMed]
3. Cheng, Y.; Ding, L. Pushing Commercialization of Perovskite Solar Cells by Improving Their Intrinsic Stability. *Energy Environ. Sci.* **2021**, *14*, 3233–3255. [CrossRef]
4. Huang, J.; Shao, Y.; Dong, Q. Organometal Trihalide Perovskite Single Crystals: A Next Wave of Materials for 25% Efficiency Photovoltaics and Applications Beyond? *J. Phys. Chem. Lett.* **2015**, *6*, 3218–3227. [CrossRef]
5. Babayigit, A.; Ethirajan, A.; Muller, M.; Conings, B. Toxicity of Organometal Halide Perovskite Solar Cells. *Nat. Mater.* **2016**, *15*, 247–251. [CrossRef] [PubMed]
6. Noel, N.K.; Stranks, S.D.; Abate, A.; Wehrenfennig, C.; Guarnera, S.; Haghighirad, A.-A.; Sadhanala, A.; Eperon, G.E.; Pathak, S.K.; Johnston, M.B.; et al. Lead-Free Organic–Inorganic Tin Halide Perovskites for Photovoltaic Applications. *Energy Environ. Sci.* **2014**, *7*, 3061–3068. [CrossRef]
7. Hao, F.; Stoumpos, C.C.; Cao, D.H.; Chang, R.P.H.; Kanatzidis, M.G. Lead-Free Solid-State Organic–Inorganic Halide Perovskite Solar Cells. *Nat. Photonics* **2014**, *8*, 489–494. [CrossRef]
8. Abdelhady, A.L.; Saidaminov, M.I.; Murali, B.; Adinolfi, V.; Voznyy, O.; Katsiev, K.; Alarousu, E.; Comin, R.; Dursun, I.; Sinatra, L.; et al. Heterovalent Dopant Incorporation for Bandgap and Type Engineering of Perovskite Crystals. *J. Phys. Chem. Lett.* **2016**, *7*, 295–301. [CrossRef]
9. Navas, J.; Sánchez-Coronilla, A.; Jesús Gallardo, J.; Hernández, N.C.; Carlos Piñero, J.; Alcántara, R.; Fernández-Lorenzo, C.; Los Santos, D.M.D.; Aguilar, T.; Martín-Calleja, J. New Insights into Organic–Inorganic Hybrid Perovskite $CH_3NH_3PbI_3$ Nanoparticles. An Experimental and Theoretical Study of Doping in Pb^{2+} Sites with Sn^{2+}, Sr^{2+}, Cd^{2+} and Ca^{2+}. *Nanoscale* **2015**, *7*, 6216–6229. [CrossRef]

10. Xu, F.; Zhang, M.; Li, Z.; Yang, X.; Zhu, R. Challenges and Perspectives toward Future Wide-Bandgap Mixed-Halide Perovskite Photovoltaics. *Adv. Energy Mater.* **2023**, *13*, 2203911. [CrossRef]
11. Zhang, F.; Yang, B.; Li, Y.; Deng, W.; He, R. Extra Long Electron–Hole Diffusion Lengths in $CH_3NH3PbI_{3-x}Cl_x$ Perovskite Single Crystals. *J. Mater. Chem. C* **2017**, *5*, 8431–8435. [CrossRef]
12. Stranks, S.D.; Eperon, G.E.; Grancini, G.; Menelaou, C.; Alcocer, M.J.P.; Leijtens, T.; Herz, L.M.; Petrozza, A.; Snaith, H.J. Electron-Hole Diffusion Lengths Exceeding 1 Micrometer in an Organometal Trihalide Perovskite Absorber. *Science* **2013**, *342*, 341–344. [CrossRef]
13. Huang, C.; Fu, N.; Liu, F.; Jiang, L.; Hao, X.; Huang, H. Highly Efficient Perovskite Solar Cells with Precursor Composition-Dependent Morphology. *Sol. Energy Mater. Sol. Cells* **2016**, *145*, 231–237. [CrossRef]
14. Yang, L.; Barrows, A.T.; Lidzey, D.G.; Wang, T. Recent Progress and Challenges of Organometal Halide Perovskite Solar Cells. *Rep. Prog. Phys.* **2016**, *79*, 026501. [CrossRef]
15. Lee, M.M.; Teuscher, J.; Miyasaka, T.; Murakami, T.N.; Snaith, H.J. Efficient Hybrid Solar Cells Based on Meso-Superstructured Organometal Halide Perovskites. *Science* **2012**, *338*, 643–647. [CrossRef] [PubMed]
16. Conings, B.; Baeten, L.; De Dobbelaere, C.; D'Haen, J.; Manca, J.; Boyen, H.-G. Perovskite-Based Hybrid Solar Cells Exceeding 10% Efficiency with High Reproducibility Using a Thin Film Sandwich Approach. *Adv. Mater.* **2014**, *26*, 2041–2046. [CrossRef]
17. Ball, J.M.; Lee, M.M.; Hey, A.; Snaith, H.J. Low-Temperature Processed Meso-Superstructured to Thin-Film Perovskite Solar Cells. *Energy Environ. Sci.* **2013**, *6*, 1739–1743. [CrossRef]
18. Eperon, G.E.; Burlakov, V.M.; Docampo, P.; Goriely, A.; Snaith, H.J. Morphological Control for High Performance, Solution-Processed Planar Heterojunction Perovskite Solar Cells. *Adv. Funct. Mater.* **2014**, *24*, 151–157. [CrossRef]
19. You, J.; Hong, Z.; Yang, Y.; Chen, Q.; Cai, M.; Song, T.-B.; Chen, C.-C.; Lu, S.; Liu, Y.; Zhou, H.; et al. Low-Temperature Solution-Processed Perovskite Solar Cells with High Efficiency and Flexibility. *ACS Nano* **2014**, *8*, 1674–1680. [CrossRef]
20. Wang, D.; Liu, Z.; Zhou, Z.; Zhu, H.; Zhou, Y.; Huang, C.; Wang, Z.; Xu, H.; Jin, Y.; Fan, B.; et al. Reproducible One-Step Fabrication of Compact $MAPbI_{3-X}Cl_x$ Thin Films Derived from Mixed-Lead-Halide Precursors. *Chem. Mater.* **2014**, *26*, 7145–7150. [CrossRef]
21. Jiang, M.; Wu, J.; Lan, F.; Tao, Q.; Gao, D.; Li, G. Enhancing the Performance of Planar Organo-Lead Halide Perovskite Solar Cells by Using a Mixed Halide Source. *J. Mater. Chem. A* **2014**, *3*, 963–967. [CrossRef]
22. Dharani, S.; Dewi, H.A.; Prabhakar, R.R.; Baikie, T.; Shi, C.; Yonghua, D.; Mathews, N.; Boix, P.P.; Mhaisalkar, S.G. Incorporation of Cl into Sequentially Deposited Lead Halide Perovskite Films for Highly Efficient Mesoporous Solar Cells. *Nanoscale* **2014**, *6*, 13854–13860. [CrossRef]
23. Docampo, P.; Hanusch, F.C.; Stranks, S.D.; Döblinger, M.; Feckl, J.M.; Ehrensperger, M.; Minar, N.K.; Johnston, M.B.; Snaith, H.J.; Bein, T. Solution Deposition-Conversion for Planar Heterojunction Mixed Halide Perovskite Solar Cells. *Adv. Energy Mater.* **2014**, *4*, 1400355. [CrossRef]
24. Dong, Q.; Yuan, Y.; Shao, Y.; Fang, Y.; Wang, Q.; Huang, J. Abnormal Crystal Growth in $CH_3NH_3PbI_{3-x}Cl_x$ Using a Multi-Cycle Solution Coating Process. *Energy Environ. Sci.* **2015**, *8*, 2464–2470. [CrossRef]
25. Chen, Y.; Chen, T.; Dai, L. Layer-by-Layer Growth of $CH_3NH_3PbI_{3-x}Cl_x$ for Highly Efficient Planar Heterojunction Perovskite Solar Cells. *Adv. Mater.* **2015**, *27*, 1053–1059. [CrossRef]
26. Liu, M.; Johnston, M.B.; Snaith, H.J. Efficient Planar Heterojunction Perovskite Solar Cells by Vapour Deposition. *Nature* **2013**, *501*, 395–398. [CrossRef]
27. Luo, P.; Liu, Z.; Xia, W.; Yuan, C.; Cheng, J.; Xu, C.; Lu, Y. Chlorine-Conducted Defect Repairment and Seed Crystal-Mediated Vapor Growth Process for Controllable Preparation of Efficient and Stable Perovskite Solar Cells. *J. Mater. Chem. A* **2015**, *3*, 22949–22959. [CrossRef]
28. Liu, D.; Wu, L.; Li, C.; Ren, S.; Zhang, J.; Li, W.; Feng, L. Controlling $CH_3NH_3PbI_{3-X}Cl_x$ Film Morphology with Two-Step Annealing Method for Efficient Hybrid Perovskite Solar Cells. *ACS Appl. Mater. Interfaces* **2015**, *7*, 16330–16337. [CrossRef] [PubMed]
29. Chen, Q.; Zhou, H.; Fang, Y.; Stieg, A.Z.; Song, T.-B.; Wang, H.-H.; Xu, X.; Liu, Y.; Lu, S.; You, J.; et al. The Optoelectronic Role of Chlorine in $CH_3NH_3PbI_3$(Cl)-Based Perovskite Solar Cells. *Nat. Commun.* **2015**, *6*, 7269. [CrossRef]
30. Li, W.; Fan, J.; Mai, Y.; Wang, L. Aquointermediate Assisted Highly Orientated Perovskite Thin Films toward Thermally Stable and Efficient Solar Cells. *Adv. Energy Mater.* **2017**, *7*, 1601433. [CrossRef]
31. Ahmadi, M.; Hsiao, Y.-C.; Wu, T.; Liu, Q.; Qin, W.; Hu, B. Effect of Photogenerated Dipoles in the Hole Transport Layer on Photovoltaic Performance of Organic–Inorganic Perovskite Solar Cells. *Adv. Energy Mater.* **2017**, *7*, 1601575. [CrossRef]
32. Liao, H.-C.; Guo, P.; Hsu, C.-P.; Lin, M.; Wang, B.; Zeng, L.; Huang, W.; Soe, C.M.M.; Su, W.-F.; Bedzyk, M.J.; et al. Enhanced Efficiency of Hot-Cast Large-Area Planar Perovskite Solar Cells/Modules Having Controlled Chloride Incorporation. *Adv. Energy Mater.* **2017**, *7*, 1601660. [CrossRef]
33. Mu, C.; Pan, J.; Feng, S.; Li, Q.; Xu, D. Quantitative Doping of Chlorine in Formamidinium Lead Trihalide ($FAPbI_{3-x}Cl_x$) for Planar Heterojunction Perovskite Solar Cells. *Adv. Energy Mater.* **2017**, *7*, 1601297. [CrossRef]

34. Qing, J.; Chandran, H.-T.; Cheng, Y.-H.; Liu, X.-K.; Li, H.-W.; Tsang, S.-W.; Lo, M.-F.; Lee, C.-S. Chlorine Incorporation for Enhanced Performance of Planar Perovskite Solar Cell Based on Lead Acetate Precursor. *ACS Appl. Mater. Interfaces* **2015**, *7*, 23110–23116. [CrossRef] [PubMed]
35. Liu, J.; Lin, J.; Xue, Q.; Ye, Q.; He, X.; Ouyang, L.; Zhuang, D.; Liao, C.; Yip, H.-L.; Mei, J.; et al. Growth and Evolution of Solution-Processed $CH_3NH_3PbI_{3-X}Cl_x$ Layer for Highly Efficient Planar-Heterojunction Perovskite Solar Cells. *J. Power Sources* **2016**, *301*, 242–250. [CrossRef]
36. Rao, H.; Ye, S.; Sun, W.; Yan, W.; Li, Y.; Peng, H.; Liu, Z.; Bian, Z.; Li, Y.; Huang, C. A 19.0% Efficiency Achieved in CuOx-Based Inverted $CH_3NH_3PbI_{3-x}Cl_x$ Solar Cells by an Effective Cl Doping Method. *Nano Energy* **2016**, *27*, 51–57. [CrossRef]
37. Islam, B.; Yanagida, M.; Shirai, Y.; Nabetani, Y.; Miyano, K. NiO_x Hole Transport Layer for Perovskite Solar Cells with Improved Stability and Reproducibility. *ACS Omega* **2017**, *2*, 2291–2299. [CrossRef] [PubMed]
38. Hu, L.; Li, M.; Yang, K.; Xiong, Z.; Yang, B.; Wang, M.; Tang, X.; Zang, Z.; Liu, X.; Li, B.; et al. PEDOT:PSS Monolayers to Enhance the Hole Extraction and Stability of Perovskite Solar Cells. *J. Mater. Chem. A* **2018**, *6*, 16583–16589. [CrossRef]
39. Peng, L.; Liu, Z. Reduce the Hysteresis Effect with the PEIE Interface Dipole Effect in the Organic-Inorganic Hybrid Perovskite $CH_3NH_3PbI_{3-X}Cl_x$ Solar Cell. *Org. Electron.* **2018**, *62*, 630–636. [CrossRef]
40. Zeng, X.; Zhou, T.; Leng, C.; Zang, Z.; Wang, M.; Hu, W.; Tang, X.; Lu, S.; Fang, L.; Zhou, M. Performance Improvement of Perovskite Solar Cells by Employing a CdSe Quantum Dot/PCBM Composite as an Electron Transport Layer. *J. Mater. Chem. A* **2017**, *5*, 17499–17505. [CrossRef]
41. Peng, L.; Xie, W.; Yang, C. Study of the Effect of DIO Additive on Charge Extraction and Recombination in Organic–Inorganic Hybrid $MAPbI_{3-x}Cl_x$ Perovskite Solar Cell. *RSC Adv.* **2018**, *70*, 40298–40307. [CrossRef]
42. Yu, H.; Zhang, Q.; Han, C.; Zhu, X.; Sun, X.; Yang, Q.; Yang, H.; Deng, L.; Zhao, F.; Wang, K.; et al. Improving Photovoltaic Performance of Inverted Planar Structure Perovskite Solar Cells via Introducing Photogenerated Dipoles in the Electron Transport Layer. *Org. Electron.* **2018**, *63*, 137–142. [CrossRef]
43. Han, C.; Yu, H.; Duan, J.; Lu, K.; Zhang, J.; Shao, M.; Hu, B. Introducing Optically Polarizable Molecules into Perovskite Solar Cells by Simultaneously Enhanced Spin–Orbital Coupling, Suppressed Non-Radiative Recombination and Improved Transport Balance towards Enhancing Photovoltaic Actions. *J. Mater. Chem. C* **2018**, *6*, 6164–6171. [CrossRef]
44. Mamun, A.A.; Ava, T.T.; Jeong, H.J.; Jeong, M.S.; Namkoong, G. A Deconvoluted PL Approach to Probe the Charge Carrier Dynamics of the Grain Interior and Grain Boundary of a Perovskite Film for Perovskite Solar Cell Applications. *Phys. Chem. Chem. Phys.* **2017**, *19*, 9143–9148. [CrossRef] [PubMed]
45. Ko, Y.; Choi, W.Y.; Yun, Y.J.; Jun, Y. A $PbI_{2-x}Cl_x$ Seed Layer for Obtaining Efficient Planar-Heterojunction Perovskite Solar Cells via an Interdiffusion Process. *Nanoscale* **2017**, *9*, 9396–9403. [CrossRef] [PubMed]
46. Park, B.; Zhang, X.; Johansson, E.M.J.; Hagfeldt, A.; Boschloo, G.; Seok, S.I.; Edvinsson, T. Analysis of Crystalline Phases and Integration Modelling of Charge Quenching Yields in Hybrid Lead Halide Perovskite Solar Cell Materials. *Nano Energy* **2017**, *40*, 596–606. [CrossRef]
47. Wang, S.; Guan, H.; Yin, Y.; Zhang, C. The Performance Improvement of Using Hole Transport Layer with Lithium and Cobalt for Inverted Planar Perovskite Solar Cell. *Coatings* **2020**, *10*, 354. [CrossRef]
48. Liu, Y.; Shin, I.; Hwang, I.-W.; Lee, J.; Kim, S.; Lee, D.Y.; Lee, S.-H.; Jang, J.-W.; Jung, Y.K.; Jeong, J.H.; et al. Effective Hot-Air Annealing for Improving the Performance of Perovskite Solar Cells. *Sol. Energy* **2017**, *146*, 359–367. [CrossRef]
49. He, T.; Liu, Z.; Zhou, Y.; Ma, H. The Stable Perovskite Solar Cell Prepared by Rapidly Annealing Perovskite Film with Water Additive in Ambient Air. *Sol. Energy Mater. Sol. Cells* **2018**, *176*, 280–287. [CrossRef]
50. Zhang, Z.L.; Men, B.Q.; Liu, Y.F.; Gao, H.P.; Mao, Y.L. Effects of Precursor Solution Composition on the Performance and I-V Hysteresis of Perovskite Solar Cells Based on $CH_3NH_3PbI_{3-x}Cl_x$. *Nanoscale Res. Lett.* **2017**, *12*, 84. [CrossRef]
51. Fan, L.; Ding, Y.; Luo, J.; Shi, B.; Yao, X.; Wei, C.; Zhang, D.; Wang, G.; Sheng, Y.; Chen, Y.; et al. Elucidating the Role of Chlorine in Perovskite Solar Cells. *J. Mater. Chem. A* **2017**, *5*, 7423–7432. [CrossRef]
52. Duy Pham, N.; Tiing Tiong, V.; Chen, P.; Wang, L.; Wilson, G.J.; Bell, J.; Wang, H. Enhanced Perovskite Electronic Properties via a Modified Lead(Ii) Chloride Lewis Acid–Base Adduct and Their Effect in High-Efficiency Perovskite Solar Cells. *J. Mater. Chem. A* **2017**, *5*, 5195–5203. [CrossRef]
53. Cao, X.; Zhi, L.; Jia, Y.; Li, Y.; Zhao, K.; Cui, X.; Ci, L.; Ding, K.; Wei, J. Enhanced Efficiency of Perovskite Solar Cells by Introducing Controlled Chloride Incorporation into MAPbI3 Perovskite Films. *Electrochim. Acta* **2018**, *275*, 1–7. [CrossRef]
54. Li, S.; He, B.; Xu, J.; Lu, H.; Jiang, J.; Zhu, J.; Kan, Z.; Zhu, L.; Wu, F. Highly Efficient Inverted Perovskite Solar Cells Incorporating P3CT-Rb as a Hole Transport Layer to Achieve a Large Open Circuit Voltage of 1.144 V. *Nanoscale* **2020**, *12*, 3686–3691. [CrossRef]
55. Jang, J.; Choe, G.; Yim, S. Effective Control of Chlorine Contents in $MAPbI_{3-x}Cl_x$ Perovskite Solar Cells Using a Single-Source Vapor Deposition and Anion-Exchange Technique. *ACS Appl. Mater. Interfaces* **2019**, *11*, 20073–20081. [CrossRef]
56. Wu, Y.; Li, X.; Fu, S.; Wan, L.; Fang, J. Efficient Methylammonium Lead Trihalide Perovskite Solar Cells with Chloroformamidinium Chloride (Cl-FACl) as an Additive. *J. Mater. Chem. A* **2019**, *7*, 8078–8084. [CrossRef]
57. Huang, L.; Cui, X.; Liu, C.; Yang, W.; Shi, W.; Lai, J.; Wang, L. Improvement on Performance of Hybrid $CH_3NH_3PbI_{3-x}Clx$ Perovskite Solar Cells Induced Sequential Deposition by Low Pressure Assisted Solution Processing. *Sol. Energy* **2020**, *199*, 826–831. [CrossRef]
58. Ngqoloda, S.; Arendse, C.J.; Guha, S.; Muller, T.F.; Klue, S.C.; Magubane, S.S.; Oliphant, C.J. Mixed-Halide Perovskites Solar Cells through PbICl and $PbCl_2$ Precursor Films by Sequential Chemical Vapor Deposition. *Sol. Energy* **2021**, *215*, 179–188. [CrossRef]

59. Siva, U.; Murugathas, T.; Yohi, S.; Natarajan, M.; Velauthapillai, D.; Ravirajan, P. Single Walled Carbon Nanotube Incorporated Titanium Dioxide and Poly(3-Hexylthiophene) as Electron and Hole Transport Materials for Perovskite Solar Cells. *Mater. Lett.* **2020**, *276*, 128174. [CrossRef]
60. Heo, J.H.; Im, S.H. Highly Reproducible, Efficient Hysteresis-Less $CH_3NH_3PbI_{3-x}Cl_x$ Planar Hybrid Solar Cells without Requiring Heat-Treatment. *Nanoscale* **2016**, *8*, 2554–2560. [CrossRef]
61. Giuliano, G.; Bonasera, A.; Scopelliti, M.; Chillura Martino, D.; Fiore, T.; Pignataro, B. Boosting the Performance of One-Step Solution-Processed Perovskite Solar Cells Using a Natural Monoterpene Alcohol as a Green Solvent Additive. *ACS Appl. Electron. Mater.* **2021**, *3*, 1813–1825. [CrossRef]
62. Wang, Y.; Chen, Q.; Fu, J.; Liu, Z.; Sun, Z.; Zhang, S.; Zhu, Y.; Jia, X.; Zhang, J.; Yuan, N.; et al. Annealing- and Doping-Free Hole Transport Material for p-i-n Perovskite Solar Cells with Efficiency Achieving over 21%. *Chem. Eng. J.* **2022**, *433*, 133265. [CrossRef]
63. Zhao, Y.; Zhu, K. CH_3NH_3Cl-Assisted One-Step Solution Growth of $CH_3NH_3PbI_3$: Structure, Charge-Carrier Dynamics, and Photovoltaic Properties of Perovskite Solar Cells. *J. Phys. Chem. C* **2014**, *118*, 9412–9418. [CrossRef]
64. Pool, V.L.; Gold-Parker, A.; McGehee, M.D.; Toney, M.F. Chlorine in $PbCl_2$-Derived Hybrid-Perovskite Solar Absorbers. *Chem. Mater.* **2015**, *27*, 7240–7243. [CrossRef]
65. Tidhar, Y.; Edri, E.; Weissman, H.; Zohar, D.; Hodes, G.; Cahen, D.; Rybtchinski, B.; Kirmayer, S. Crystallization of Methyl Ammonium Lead Halide Perovskites: Implications for Photovoltaic Applications. *J. Am. Chem. Soc.* **2014**, *136*, 13249–13256. [CrossRef]
66. Colella, S.; Mosconi, E.; Pellegrino, G.; Alberti, A.; Guerra, V.L.P.; Masi, S.; Listorti, A.; Rizzo, A.; Condorelli, G.G.; De Angelis, F.; et al. Elusive Presence of Chloride in Mixed Halide Perovskite Solar Cells. *J. Phys. Chem. Lett.* **2014**, *5*, 3532–3538. [CrossRef] [PubMed]
67. Unger, E.L.; Bowring, A.R.; Tassone, C.J.; Pool, V.L.; Gold-Parker, A.; Cheacharoen, R.; Stone, K.H.; Hoke, E.T.; Toney, M.F.; McGehee, M.D. Chloride in Lead Chloride-Derived Organo-Metal Halides for Perovskite-Absorber Solar Cells. *Chem. Mater.* **2014**, *26*, 7158–7165. [CrossRef]
68. Salim, T.; Sun, S.; Abe, Y.; Krishna, A.; Grimsdale, A.C.; Lam, Y.M. Perovskite-Based Solar Cells: Impact of Morphology and Device Architecture on Device Performance. *J. Mater. Chem. A* **2015**, *3*, 8943–8969. [CrossRef]
69. Qiao, W.-C.; Yang, J.; Dong, W.; Yang, G.; Bao, Q.; Huang, R.; Wang, X.L.; Yao, Y.-F. Metastable Alloying Structures in $MAPbI_{3-x}Cl_x$ Crystals. *NPG Asia Mater.* **2020**, *12*, 68. [CrossRef]
70. Bartel, C.J.; Sutton, C.; Goldsmith, B.R.; Ouyang, R.; Musgrave, C.B.; Ghiringhelli, L.M.; Scheffler, M. New Tolerance Factor to Predict the Stability of Perovskite Oxides and Halides. *Sci. Adv.* **2019**, *5*, eaav0693. [CrossRef] [PubMed]
71. McLeod, J.A.; Wu, Z.; Sun, B.; Liu, L. The Influence of the I/Cl Ratio on the Performance of $CH_3NH_3PbI_{3-x}Cl_x$-Based Solar Cells: Why Is CH_3NH_3I:PbCl2=3:1 the "Magic" Ratio? *Nanoscale* **2016**, *8*, 6361–6368. [CrossRef]
72. Xu, F.; Zhang, T.; Li, G.; Zhao, Y. Synergetic Effect of Chloride Doping and $CH_3NH_3PbCl_3$ on $CH_3NH_3PbI_{3-x}Cl_x$ Perovskite-Based Solar Cells. *ChemSusChem* **2017**, *10*, 2365–2369. [CrossRef] [PubMed]
73. Bouchard, M.; Hilhorst, J.; Pouget, S.; Alam, F.; Mendez, M.; Djurado, D.; Aldakov, D.; Schülli, T.; Reiss, P. Direct Evidence of Chlorine-Induced Preferential Crystalline Orientation in Methylammonium Lead Iodide Perovskites Grown on TiO2. *J. Phys. Chem. C* **2017**, *121*, 7596–7602. [CrossRef]
74. Kim, H.-S.; Hagfeldt, A.; Park, N.-G. Morphological and Compositional Progress in Halide Perovskite Solar Cells. *Chem. Commun.* **2019**, *55*, 1192–1200. [CrossRef] [PubMed]
75. Williams, S.T.; Zuo, F.; Chueh, C.-C.; Liao, C.-Y.; Liang, P.-W.; Jen, A.K.-Y. Role of Chloride in the Morphological Evolution of Organo-Lead Halide Perovskite Thin Films. *ACS Nano* **2014**, *8*, 10640–10654. [CrossRef] [PubMed]
76. Dar, M.I.; Arora, N.; Gao, P.; Ahmad, S.; Grätzel, M.; Nazeeruddin, M.K. Investigation Regarding the Role of Chloride in Organic–Inorganic Halide Perovskites Obtained from Chloride Containing Precursors. *Nano Lett.* **2014**, *14*, 6991–6996. [CrossRef]
77. Colella, S.; Mosconi, E.; Fedeli, P.; Listorti, A.; Gazza, F.; Orlandi, F.; Ferro, P.; Besagni, T.; Rizzo, A.; Calestani, G.; et al. $MAPbI_{3-x}Cl_x$ Mixed Halide Perovskite for Hybrid Solar Cells: The Role of Chloride as Dopant on the Transport and Structural Properties. *Chem. Mater.* **2013**, *25*, 4613–4618. [CrossRef]
78. Yantara, N.; Yanan, F.; Shi, C.; Dewi, H.A.; Boix, P.P.; Mhaisalkar, S.G.; Mathews, N. Unravelling the Effects of Cl Addition in Single Step $CH_3NH_3PbI_3$ Perovskite Solar Cells. *Chem. Mater.* **2015**, *27*, 2309–2314. [CrossRef]
79. Tombe, S.; Adam, G.; Heilbrunner, H.; Yumusak, C.; Apaydin, D.H.; Hailegnaw, B.; Ulbricht, C.; Arendse, C.J.; Langhals, H.; Iwuohaa, E.; et al. The Influence of Perovskite Precursor Composition on the Morphology and Photovoltaic Performance of Mixed Halide $MAPbI_{3-X}Cl_x$ Solar Cells. *Sol. Energy* **2018**, *163*, 215–223. [CrossRef]
80. Li, T.; Pan, Y.; Wang, Z.; Xia, Y.; Chen, Y.; Huang, W. Additive Engineering for Highly Efficient Organic–Inorganic Halide Perovskite Solar Cells: Recent Advances and Perspectives. *J. Mater. Chem. A* **2017**, *5*, 12602–12652. [CrossRef]
81. Zhang, F.; Zhu, K. Additive Engineering for Efficient and Stable Perovskite Solar Cells. *Adv. Energy Mater.* **2020**, *10*, 1902579. [CrossRef]
82. Pereyra, C.; Xie, H.; Lira-Cantu, M. Additive Engineering for Stable Halide Perovskite Solar Cells. *J. Energy Chem.* **2021**, *60*, 599–634. [CrossRef]

83. Mahapatra, A.; Prochowicz, D.; Tavakoli, M.M.; Trivedi, S.; Kumar, P.; Yadav, P.K. A Review of Aspects of Additive Engineering in Perovskite Solar Cells. *J. Mater. Chem. A* **2020**, *8*, 27–54. [CrossRef]
84. Wang, L.; Liu, G.; Xi, X.; Yang, G.; Hu, L.; Zhu, B.; He, Y.; Liu, Y.; Qian, H.; Zhang, S.; et al. Annealing Engineering in the Growth of Perovskite Grains. *Crystals* **2022**, *12*, 894. [CrossRef]
85. Dong, H.; Pang, S.; He, F.; Yang, H.; Zhu, W.; Chen, D.; Xi, H.; Zhang, J.; Hao, Y.; Zhang, C. Annealing-Free, High-Performance Perovskite Solar Cells by Controlling Crystallization via Guanidinium Cation Doping. *Sol. RRL* **2021**, *5*, 2100097. [CrossRef]
86. Dubey, A.; Adhikari, N.; Mabrouk, S.; Wu, F.; Chen, K.; Yang, S.; Qiao, Q. A Strategic Review on Processing Routes towards Highly Efficient Perovskite Solar Cells. *J. Mater. Chem. A* **2018**, *6*, 2406–2431. [CrossRef]
87. Cao, X.; Zhi, L.; Jia, Y.; Li, Y.; Zhao, K.; Cui, X.; Ci, L.; Zhuang, D.; Wei, J. A Review of the Role of Solvents in Formation of High-Quality Solution-Processed Perovskite Films. *ACS Appl. Mater. Interfaces* **2019**, *11*, 7639–7654. [CrossRef] [PubMed]
88. Chao, L.; Niu, T.; Gao, W.; Ran, C.; Song, L.; Chen, Y.; Huang, W. Solvent Engineering of the Precursor Solution toward Large-Area Production of Perovskite Solar Cells. *Adv. Mater.* **2021**, *33*, 2005410. [CrossRef]
89. Mehdi, H.; Mhamdi, A.; Bouazizi, A. Effect of Perovskite Precursor Ratios and Solvents Volume on the Efficiency of $MAPbI_{3-X}Cl_x$ Mixed Halide Perovskite Solar Cells. *Mater. Sci. Semicond. Process.* **2020**, *109*, 104915. [CrossRef]
90. Buin, A.; Comin, R.; Xu, J.; Ip, A.H.; Sargent, E.H. Halide-Dependent Electronic Structure of Organolead Perovskite Materials. *Chem. Mater.* **2015**, *27*, 4405–4412. [CrossRef]
91. Tong, G.; Son, D.-Y.; Ono, L.K.; Liu, Y.; Hu, Y.; Zhang, H.; Jamshaid, A.; Qiu, L.; Liu, Z.; Qi, Y. Scalable Fabrication of >90 cm^2 Perovskite Solar Modules with >1000 h Operational Stability Based on the Intermediate Phase Strategy. *Adv. Energy Mater.* **2021**, *11*, 2003712. [CrossRef]
92. Niu, G.; Guo, X.; Wang, L. Review of Recent Progress in Chemical Stability of Perovskite Solar Cells. *J. Mater. Chem. A* **2015**, *3*, 8970–8980. [CrossRef]
93. Liu, Y.; Feng, K.; Hsieh, R.-H.; Mo, X. $CH_3NH_3PbIxCl_{(3-x)}$ Thin Film Prepared by Vapor Transfer Method for Perovskite Solar Cells. *Mater. Lett.* **2019**, *239*, 163–166. [CrossRef]
94. Grätzel, M. The Light and Shade of Perovskite Solar Cells. *Nat. Mater.* **2014**, *13*, 838–842. [CrossRef] [PubMed]
95. Dualeh, A.; Tétreault, N.; Moehl, T.; Gao, P.; Nazeeruddin, M.K.; Grätzel, M. Effect of Annealing Temperature on Film Morphology of Organic–Inorganic Hybrid Pervoskite Solid-State Solar Cells. *Adv. Funct. Mater.* **2014**, *24*, 3250–3258. [CrossRef]
96. Tan, K.W.; Moore, D.T.; Saliba, M.; Sai, H.; Estroff, L.A.; Hanrath, T.; Snaith, H.J.; Wiesner, U. Thermally Induced Structural Evolution and Performance of Mesoporous Block Copolymer-Directed Alumina Perovskite Solar Cells. *ACS Nano* **2014**, *8*, 4730–4739. [CrossRef]
97. Yu, H.; Wang, F.; Xie, F.; Li, W.; Chen, J.; Zhao, N. The Role of Chlorine in the Formation Process of "$CH_3NH_3PbI_{3-X}Cl_x$" Perovskite. *Adv. Funct. Mater.* **2014**, *24*, 7102–7108. [CrossRef]
98. Ralaiarisoa, M.; Busby, Y.; Frisch, J.; Salzmann, I.; Pireaux, J.-J.; Koch, N. Correlation of Annealing Time with Crystal Structure, Composition, and Electronic Properties of $CH_3NH_3PbI_{3-x}Cl_x$ Mixed-Halide Perovskite Films. *Phys. Chem. Chem. Phys.* **2016**, *19*, 828–836. [CrossRef]
99. Cronin, H.M.; Jayawardena, K.D.G.I.; Stoeva, Z.; Shkunov, M.; Silva, S.R.P. Effects of Ambient Humidity on the Optimum Annealing Time of Mixed-Halide Perovskite Solar Cells. *Nanotechnology* **2017**, *28*, 114004. [CrossRef]
100. You, J.; Yang, Y.; Hong, Z.; Song, T.-B.; Meng, L.; Liu, Y.; Jiang, C.; Zhou, H.; Chang, W.-H.; Li, G.; et al. Moisture Assisted Perovskite Film Growth for High Performance Solar Cells. *Appl. Phys. Lett.* **2014**, *105*, 183902. [CrossRef]
101. Eperon, G.E.; Habisreutinger, S.N.; Leijtens, T.; Bruijnaers, B.J.; van Franeker, J.J.; de Quilettes, D.W.; Pathak, S.; Sutton, R.J.; Grancini, G.; Ginger, D.S.; et al. The Importance of Moisture in Hybrid Lead Halide Perovskite Thin Film Fabrication. *ACS Nano* **2015**, *9*, 9380–9393. [CrossRef] [PubMed]
102. Xie, F.X.; Zhang, D.; Su, H.; Ren, X.; Wong, K.S.; Grätzel, M.; Choy, W.C.H. Vacuum-Assisted Thermal Annealing of $CH_3NH_3PbI_3$ for Highly Stable and Efficient Perovskite Solar Cells. *ACS Nano* **2015**, *9*, 639–646. [CrossRef]
103. Xiao, Z.; Dong, Q.; Bi, C.; Shao, Y.; Yuan, Y.; Huang, J. Solvent Annealing of Perovskite-Induced Crystal Growth for Photovoltaic-Device Efficiency Enhancement. *Adv. Mater.* **2014**, *26*, 6503–6509. [CrossRef]
104. Webb, T.; Sweeney, S.J.; Zhang, W. Device Architecture Engineering: Progress toward Next Generation Perovskite Solar Cells. *Adv. Funct. Mater.* **2021**, *31*, 2103121. [CrossRef]
105. Dahal, B.; Li, W. Configuration of Methylammonium Lead Iodide Perovskite Solar Cell and Its Effect on the Device's Performance: A Review. *Adv. Mater. Interfaces* **2022**, *9*, 2200042. [CrossRef]
106. Docampo, P.; Ball, J.M.; Darwich, M.; Eperon, G.E.; Snaith, H.J. Efficient Organometal Trihalide Perovskite Planar-Heterojunction Solar Cells on Flexible Polymer Substrates. *Nat. Commun.* **2013**, *4*, 2761. [CrossRef] [PubMed]
107. Kim, J.Y.; Lee, J.-W.; Jung, H.S.; Shin, H.; Park, N.-G. High-Efficiency Perovskite Solar Cells. *Chem. Rev.* **2020**, *120*, 7867–7918. [CrossRef]
108. Yin, W.-J.; Yang, J.-H.; Kang, J.; Yan, Y.; Wei, S.-H. Halide Perovskite Materials for Solar Cells: A Theoretical Review. *J. Mater. Chem. A* **2015**, *3*, 8926–8942. [CrossRef]
109. Ono, L.K.; Qi, Y.; Liu, S. Progress toward Stable Lead Halide Perovskite Solar Cells. *JOULE* **2018**, *2*, 1961–1990. [CrossRef]

110. Li, N.; Niu, X.; Chen, Q.; Zhou, H. Towards Commercialization: The Operational Stability of Perovskite Solar Cells. *Chem. Soc. Rev.* **2020**, *49*, 8235–8286. [CrossRef]
111. Cheng, Y.; So, F.; Tsang, S.-W. Progress in Air-Processed Perovskite Solar Cells: From Crystallization to Photovoltaic Performance. *Mater. Horiz.* **2019**, *6*, 1611–1624. [CrossRef]
112. Sahare, S.; Pham, H.D.; Angmo, D.; Ghoderao, P.; MacLeod, J.; Khan, S.B.; Lee, S.-L.; Singh, S.P.; Sonar, P. Emerging Perovskite Solar Cell Technology: Remedial Actions for the Foremost Challenges. *Adv. Energy Mater.* **2021**, *11*, 2101085. [CrossRef]
113. Wali, Q.; Iftikhar, F.J.; Khan, M.E.; Ullah, A.; Iqbal, Y.; Jose, R. Advances in Stability of Perovskite Solar Cells. *Org. Electron.* **2020**, *78*, 105590. [CrossRef]
114. Wang, R.; Mujahid, M.; Duan, Y.; Wang, Z.-K.; Xue, J.; Yang, Y. A Review of Perovskites Solar Cell Stability. *Adv. Funct. Mater.* **2019**, *29*, 1808843. [CrossRef]
115. Klein-Kedem, N.; Cahen, D.; Hodes, G. Effects of Light and Electron Beam Irradiation on Halide Perovskites and Their Solar Cells. *Acc. Chem. Res.* **2016**, *49*, 347–354. [CrossRef]
116. Younas, M.; Kandiel, T.A.; Rinaldi, A.; Peng, Q.; Al-Saadi, A.A. Ambient-Environment Processed Perovskite Solar Cells: A Review. *Mater. Today Phys.* **2021**, *21*, 100557. [CrossRef]
117. Sheikh, A.D.; Bera, A.; Haque, M.A.; Rakhi, R.B.; Gobbo, S.D.; Alshareef, H.N.; Wu, T. Atmospheric Effects on the Photovoltaic Performance of Hybrid Perovskite Solar Cells. *Sol. Energy Mater. Sol. Cells* **2015**, *137*, 6–14. [CrossRef]
118. Kazim, S.; Nazeeruddin, M.K.; Grätzel, M.; Ahmad, S. Perovskite as Light Harvester: A Game Changer in Photovoltaics. *Angew. Chem. Int. Ed.* **2014**, *53*, 2812–2824. [CrossRef] [PubMed]
119. Tiep, N.H.; Ku, Z.; Fan, H.J. Recent Advances in Improving the Stability of Perovskite Solar Cells. *Adv. Energy Mater.* **2016**, *6*, 1501420. [CrossRef]
120. Zhao, X.; Park, N.-G. Stability Issues on Perovskite Solar Cells. *Photonics* **2015**, *2*, 1139–1151. [CrossRef]
121. Zhang, C.-X.; Shen, T.; Guo, D.; Tang, L.-M.; Yang, K.; Deng, H.-X. Reviewing and Understanding the Stability Mechanism of Halide Perovskite Solar Cells. *InfoMat* **2020**, *2*, 1034–1056. [CrossRef]
122. Zhang, Y.; Kirs, A.; Ambroz, F.; Lin, C.-T.; Bati, A.S.R.; Parkin, I.P.; Shapter, J.G.; Batmunkh, M.; Macdonald, T.J. Ambient Fabrication of Organic–Inorganic Hybrid Perovskite Solar Cells. *Small Methods* **2021**, *5*, 2000744. [CrossRef]
123. Asghar, M.I.; Zhang, J.; Wang, H.; Lund, P.D. Device Stability of Perovskite Solar Cells—A Review. *Renew. Sustain. Energy Rev.* **2017**, *77*, 131–146. [CrossRef]
124. Ueoka, N.; Oku, T. Stability Characterization of PbI_2-Added $CH_3NH_3PbI_{3-X}Cl_x$ Photovoltaic Devices. *ACS Appl. Mater. Interfaces* **2018**, *10*, 44443–44451. [CrossRef]
125. Saidaminov, M.I.; Kim, J.; Jain, A.; Quintero-Bermudez, R.; Tan, H.; Long, G.; Tan, F.; Johnston, A.; Zhao, Y.; Voznyy, O.; et al. Suppression of Atomic Vacancies via Incorporation of Isovalent Small Ions to Increase the Stability of Halide Perovskite Solar Cells in Ambient Air. *Nat. Energy* **2018**, *3*, 648–654. [CrossRef]
126. Lee, J.-W.; Kim, H.-S.; Park, N.-G. Lewis Acid–Base Adduct Approach for High Efficiency Perovskite Solar Cells. *Acc. Chem. Res.* **2016**, *49*, 311–319. [CrossRef]
127. Odunmbaku, G.O.; Chen, S.; Guo, B.; Zhou, Y.; Ouedraogo, N.A.N.; Zheng, Y.; Li, J.; Li, M.; Sun, K. Recombination Pathways in Perovskite Solar Cells. *Adv. Mater. Interfaces* **2022**, *9*, 2102137. [CrossRef]
128. Zhang, T.; Hu, C.; Yang, S. Ion Migration: A "Double-Edged Sword" for Halide-Perovskite-Based Electronic Devices. *Small Methods* **2020**, *4*, 1900552. [CrossRef]
129. Zhang, Y.; Liu, M.; Eperon, G.E.; Leijtens, T.C.; McMeekin, D.; Saliba, M.; Zhang, W.; de Bastiani, M.; Petrozza, A.; Herz, L.M.; et al. Charge Selective Contacts, Mobile Ions and Anomalous Hysteresis in Organic–Inorganic Perovskite Solar Cells. *Mater. Horiz.* **2015**, *2*, 315–322. [CrossRef]
130. Li, Z.; Xiao, C.; Yang, Y.; Harvey, S.P.; Kim, D.H.; Christians, J.A.; Yang, M.; Schulz, P.; Nanayakkara, S.U.; Jiang, C.-S.; et al. Extrinsic Ion Migration in Perovskite Solar Cells. *Energy Environ. Sci.* **2017**, *10*, 1234–1242. [CrossRef]
131. Yuan, Y.; Chae, J.; Shao, Y.; Wang, Q.; Xiao, Z.; Centrone, A.; Huang, J. Photovoltaic Switching Mechanism in Lateral Structure Hybrid Perovskite Solar Cells. *Adv. Energy Mater.* **2015**, *5*, 1500615. [CrossRef]
132. Yuan, Y.; Wang, Q.; Shao, Y.; Lu, H.; Li, T.; Gruverman, A.; Huang, J. Electric-Field-Driven Reversible Conversion between Methylammonium Lead Triiodide Perovskites and Lead Iodide at Elevated Temperatures. *Adv. Energy Mater.* **2016**, *6*, 1501803. [CrossRef]
133. Wu, F.; Pathak, R.; Qiao, Q. Origin and Alleviation of J-V Hysteresis in Perovskite Solar Cells: A Short Review. *Catal. Today* **2021**, *374*, 86–101. [CrossRef]
134. Duan, L.; Uddin, A. Defects and Stability of Perovskite Solar Cells: A Critical Analysis. *Mater. Chem. Front.* **2022**, *6*, 400–417. [CrossRef]
135. McGehee, M.D. Continuing to Soar. *Nat. Mater.* **2014**, *13*, 845–846. [CrossRef]
136. Liu, P.; Wang, W.; Liu, S.; Yang, H.; Shao, Z. Fundamental Understanding of Photocurrent Hysteresis in Perovskite Solar Cells. *Adv. Energy Mater.* **2019**, *9*, 1803017. [CrossRef]
137. Elumalai, N.K.; Uddin, A. Hysteresis in Organic-Inorganic Hybrid Perovskite Solar Cells. *Sol. Energy Mater. Sol. Cells* **2016**, *157*, 476–509. [CrossRef]

138. Xiao, J.-W.; Shi, C.; Zhou, C.; Zhang, D.; Li, Y.; Chen, Q. Contact Engineering: Electrode Materials for Highly Efficient and Stable Perovskite Solar Cells. *Sol. RRL* **2017**, *1*, 1700082. [CrossRef]
139. Leijtens, T.; Eperon, G.E.; Pathak, S.; Abate, A.; Lee, M.M.; Snaith, H.J. Overcoming Ultraviolet Light Instability of Sensitized TiO_2 with Meso-Superstructured Organometal Tri-Halide Perovskite Solar Cells. *Nat. Commun.* **2013**, *4*, 2885. [CrossRef]
140. Guo, S.; Sun, X.; Ding, C.; Huang, R.; Tan, M.; Zhang, L.; Luo, Q.; Li, F.; Jin, J.; Ma, C.-Q. Non-Uniform Chemical Corrosion of Metal Electrode of p–i–n Type of Perovskite Solar Cells Caused by the Diffusion of CH_3NH_3I. *Energy Technol.* **2020**, *8*, 2000250. [CrossRef]
141. Wang, Z.; Shi, Z.; Li, T.; Chen, Y.; Huang, W. Stability of Perovskite Solar Cells: A Prospective on the Substitution of the A Cation and X Anion. *Angew. Chem. Int. Ed.* **2017**, *56*, 1190–1212. [CrossRef] [PubMed]
142. Conings, B.; Babayigit, A.; Vangerven, T.; D'Haen, J.; Manca, J.; Boyen, H.-G. The Impact of Precursor Water Content on Solution-Processed Organometal Halide Perovskite Films and Solar Cells. *J. Mater. Chem. A* **2015**, *3*, 19123–19128. [CrossRef]
143. Chen, B.; Wang, S.; Song, Y.; Li, C.; Hao, F. A Critical Review on the Moisture Stability of Halide Perovskite Films and Solar Cells. *Chem. Eng. J.* **2022**, *430*, 132701. [CrossRef]
144. Christians, J.A.; Miranda Herrera, P.A.; Kamat, P.V. Transformation of the Excited State and Photovoltaic Efficiency of $CH_3NH_3PbI_3$ Perovskite upon Controlled Exposure to Humidified Air. *J. Am. Chem. Soc.* **2015**, *137*, 1530–1538. [CrossRef]
145. Kim, H.-S.; Seo, J.-Y.; Park, N.-G. Material and Device Stability in Perovskite Solar Cells. *ChemSusChem* **2016**, *9*, 2528–2540. [CrossRef]
146. Ono, L.K.; Juarez-Perez, E.J.; Qi, Y. Progress on Perovskite Materials and Solar Cells with Mixed Cations and Halide Anions. *ACS Appl. Mater. Interfaces* **2017**, *9*, 30197–30246. [CrossRef] [PubMed]
147. Montecucco, R.; Quadrivi, E.; Po, R.; Grancini, G. All-Inorganic Cesium-Based Hybrid Perovskites for Efficient and Stable Solar Cells and Modules. *Adv. Energy Mater.* **2021**, *11*, 2100672. [CrossRef]
148. Tian, J.; Xue, Q.; Yao, Q.; Li, N.; Brabec, C.J.; Yip, H.-L. Inorganic Halide Perovskite Solar Cells: Progress and Challenges. *Adv. Energy Mater.* **2020**, *10*, 2000183. [CrossRef]
149. Chen, J.; Choy, W.C.H. Efficient and Stable All-Inorganic Perovskite Solar Cells. *Sol. RRL* **2020**, *4*, 2000408. [CrossRef]
150. Tai, Q.; Tang, K.-C.; Yan, F. Recent Progress of Inorganic Perovskite Solar Cells. *Energy Environ. Sci.* **2019**, *12*, 2375–2405. [CrossRef]
151. Li, B.; Fu, L.; Li, S.; Li, H.; Pan, L.; Wang, L.; Chang, B.; Yin, L. Pathways toward High-Performance Inorganic Perovskite Solar Cells: Challenges and Strategies. *J. Mater. Chem. A* **2019**, *7*, 20494–20518. [CrossRef]
152. Maafa, I.M. All-Inorganic Perovskite Solar Cells: Recent Advancements and Challenges. *Nanomaterials* **2022**, *12*, 1651. [CrossRef]
153. Conings, B.; Drijkoningen, J.; Gauquelin, N.; Babayigit, A.; D'Haen, J.; D'Olieslaeger, L.; Ethirajan, A.; Verbeeck, J.; Manca, J.; Mosconi, E.; et al. Intrinsic Thermal Instability of Methylammonium Lead Trihalide Perovskite. *Adv. Energy Mater.* **2015**, *5*, 1500477. [CrossRef]
154. Chae, J.; Dong, Q.; Huang, J.; Centrone, A. Chloride Incorporation Process in CH3NH3PbI3–XClx Perovskites via Nanoscale Bandgap Maps. *Nano Lett.* **2015**, *15*, 8114–8121. [CrossRef]
155. Wei, J.; Wang, Q.; Huo, J.; Gao, F.; Gan, Z.; Zhao, Q.; Li, H. Mechanisms and Suppression of Photoinduced Degradation in Perovskite Solar Cells. *Adv. Energy Mater.* **2021**, *11*, 2002326. [CrossRef]
156. Xu, J.; Boyd, C.C.; Yu, Z.J.; Palmstrom, A.F.; Witter, D.J.; Larson, B.W.; France, R.M.; Werner, J.; Harvey, S.P.; Wolf, E.J.; et al. Triple-Halide Wide–Band Gap Perovskites with Suppressed Phase Segregation for Efficient Tandems. *Science* **2020**, *367*, 1097–1104. [CrossRef]
157. Ueoka, N.; Oku, T.; Ohishi, Y.; Tanaka, H.; Suzuki, A. Effects of Excess PbI_2 Addition to $CH_3NH_3PbI_{3-x}Cl_x$ Perovskite Solar Cells. *Chem. Lett.* **2018**, *47*, 528–531. [CrossRef]
158. Ranjan, R.; Ranjan, S.; Monalisa, M.; Nalwa, K.S.; Singh, A.; Garg, A.; Gupta, R.K. Enhanced Thermal and Moisture Stability via Dual Additives Approach in Methylammonium Lead Iodide Based Planar Perovskite Solar Cells. *Sol. Energy* **2021**, *225*, 200–210. [CrossRef]
159. Zhang, Y.; Li, Y.; Zhang, L.; Hu, H.; Tang, Z.; Xu, B.; Park, N.-G. Propylammonium Chloride Additive for Efficient and Stable FAPbI3 Perovskite Solar Cells. *Adv. Energy Mater.* **2021**, *11*, 2102538. [CrossRef]
160. Oku, T.; Ohishi, Y. Effects of Annealing on $CH_3NH_3PbI_3$(Cl) Perovskite Photovoltaic Devices. *J. Ceram. Soc. Jpn.* **2018**, *126*, 56–60. [CrossRef]
161. Scalon, L.; Szostak, R.; Araújo, F.L.; Adriani, K.F.; Silveira, J.F.R.V.; Oliveira, W.X.C.; Da Silva, J.L.F.; Oliveira, C.C.; Nogueira, A.F. Improving the Stability and Efficiency of Perovskite Solar Cells by a Bidentate Anilinium Salt. *JACS Au* **2022**, *2*, 1306–1312. [CrossRef] [PubMed]
162. Lee, S.; Park, J.H.; Lee, B.R.; Jung, E.D.; Yu, J.C.; Di Nuzzo, D.; Friend, R.H.; Song, M.H. Amine-Based Passivating Materials for Enhanced Optical Properties and Performance of Organic–Inorganic Perovskites in Light-Emitting Diodes. *J. Phys. Chem. Lett.* **2017**, *8*, 1784–1792. [CrossRef] [PubMed]
163. Zhang, H.; Ren, X.; Chen, X.; Mao, J.; Cheng, J.; Zhao, Y.; Liu, Y.; Milic, J.; Yin, W.-J.; Grätzel, M.; et al. Improving the Stability and Performance of Perovskite Solar Cells via Off-the-Shelf Post-Device Ligand Treatment. *Energy Environ. Sci.* **2018**, *11*, 2253–2262. [CrossRef]

164. Gharahcheshmeh, M.H.; Tavakoli, M.M.; Gleason, E.F.; Robinson, M.T.; Kong, J.; Gleason, K.K. Tuning, Optimization, and Perovskite Solar Cell Device Integration of Ultrathin Poly(3,4-Ethylene Dioxythiophene) Films via a Single-Step All-Dry Process. *Sci. Adv.* **2019**, *5*, eaay0414. [CrossRef] [PubMed]
165. Chang, X.; Li, W.; Chen, H.; Zhu, L.; Liu, H.; Geng, H.; Xiang, S.; Liu, J.; Zheng, X.; Yang, Y.; et al. Colloidal Precursor-Induced Growth of Ultra-Even $CH_3NH_3PbI_3$ for High-Performance Paintable Carbon-Based Perovskite Solar Cells. *ACS Appl. Mater. Interfaces* **2016**, *8*, 30184–30192. [CrossRef]